# Idealised tidal dynamics in an estuary with a horizontally movable time dependent barrier

## A contribution to one of the possible solutions of the sludge problem in the Eems estuary

by

M.M. de Jongh

to obtain the degree of Bachelor of Science
at the Delft University of Technology.

Student number: 4393643
Project duration: September 16, 2019 – March 5, 2020
Thesis committee: Dr. H. M. Schuttelaars, TU Delft, supervisor
Dr. S. R. de Roode, TU Delft, supervisor
Dr. F. J. Vermolen, TU Delft
Dr. J. M. Thijssen, TU Delft



TU Delft

# Contents

# 1 Introduction

In this thesis the hydrodynamic behaviour of an idealised relatively short tidal estuary is studied using a cross-sectionally averaged model, i.e. a one dimensional model. The geometry of the estuary is simplified and only the hydrodynamic processes are considered. This model is used to gain insight in the behaviour of currents and water levels influenced by a movable barrier situated in the estuary. It is investigated whether shifting the motion of the barrier in time influences the sedimentation in the embayment.

In the next section the basic properties and aspects of estuaries are explained. After this, the importance of estuaries is emphasized. In section 1.2 current research on this topic and the fundaments leading to this thesis are presented, followed by the research questions and open problems to be investigated.

## 1.1. Estuaries

An estuary is defined as a partially enclosed coastal body of brackish water with one or more rivers or streams flowing into it, and with a free connection to the open sea. The water motions are predominantly driven by tides (Pritchard, 1963). The typical length of an estuary can vary from tens to a few hundred kilometers. In section 1.1.1 the water motion, with a focus on tidal dynamics, will be discussed.

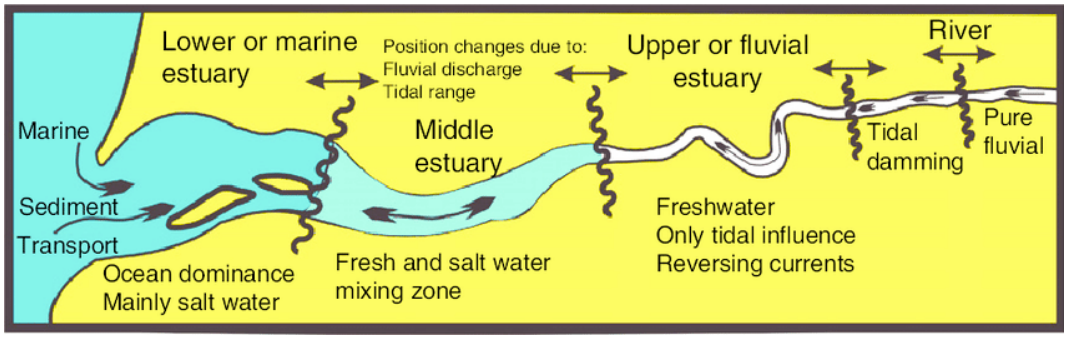


Figure 1.1: Schematic figure of an estuary. The properties change while going stream upward. The connection to the open sea mainly dominates the water motion in estuaries.

### 1.1.1. Water motion

The water movement and sea surface elevation in estuaries is highly determined by the tides that force the water at the seaward boundary and the dynamics in the estuary. Tides are the periodic rise and fall of the surface water caused by the gravitational force of the moon and the sun and by the rotation of the earth. The movements of the solar system that influence the tides are predictable (Gerkema, 2019). However, other influences such as the atmospheric pressures are only predictable to a certain extent. As tides change, the tidal waves move along the coast, as shown in figure (1.2).

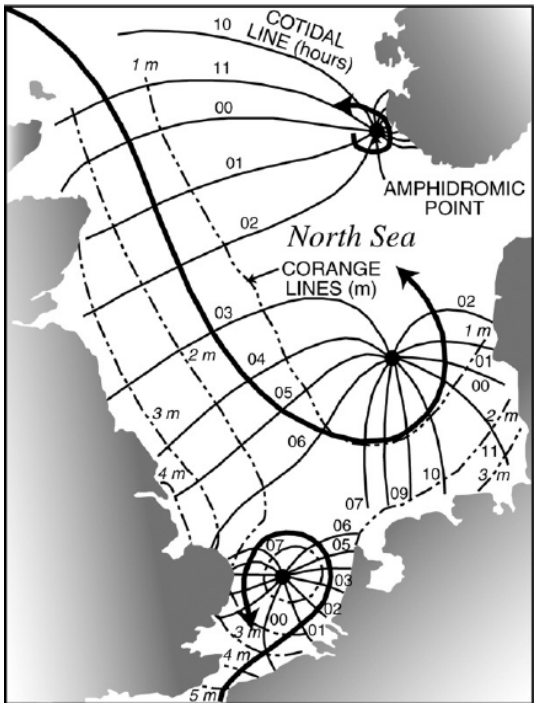


Figure 1.2: Figure of a amphidromic system for the first tide (M2): tidal waves move along the shore lines located in the north sea. The lines indicate times of high water. This figure is a modified version from Dalrymple (1992).

Tides strongly impact coastal areas and estuaries. The water motion in these basins and estuaries can resonate, leading up to a great difference in low and high tide with extraordinary currents (de Swart, 2009). These currents result in enhanced sediment transport. In many estuaries, regions are found with sediment concentrations exceeding those directly upstream or downstream. The region where the highest sediment concentration is found is called the estuarine turbidity maximum.

### 1.1.2. Functions of an estuary

Estuaries are highly important geological areas on multiple aspects. Because they connect the land and the open sea, a lot of demographic and industrial activities take place in these regions. Countless human activities are concentrated in these areas, such as fishing, recreation, sand extraction, etc. On the other hand, the large environmental variety (i.e. difference of salinity, ebb-flood difference) results in a broad and delicate biodiversity (De Vriend et al., 2002). It is the breeding place, nursery ground and resting place for fish, migratory birds and many other species. The mixing of seawater and freshwater provides high levels of nutrients both in the water column and in sediment, making estuaries among the most productive natural habitats in the world (McLusky and Elliott, 2004).

An example estuary is located between the Netherlands and Germany: the Dollar-Eems estuary. German and Dutch authorities have started to develop an integral management plan to improve the balance between economic and ecological aspects on this territory (Altenburg & Wymenga, 2002). An example of the economic importance is for instance the accessibility of the port of Eemshaven and the industrial land upstream in Germany. Here a assembling dock for cruise ships is stationed, whose revenue performance highly depends on accessibility to the open sea.

**Human interference** Present-day a lot of dredging is performed in this area. Two significant reasons are the increase in size of the ships combined with the sedimentation of sludge in the past decennia. Apart from the huge costs, this dredging causes severe consequences on the ecology, directly but also indirectly. Channeling of the waterways in estuaries and in the river Ems results in changing currents, changes in erosion and sedimentation of sludge in the system; higher turbidity causes an increase of the sludge concentrations (de Jonge, 1983, 2000; Schuttelaars et al., 2013, de Jonge et al., 2014). Cloudiness formed from the sludge causes a threat for the biodiversity and the carrying capacity of the estuary (Taal et. al, 2015).

For this reason an ecological impulse was given to the entire Eems regions. In order to achieve improvement of the ecology within the Eems estuary, various approaches are proposed. One of these measures is to minimalize the sedimentation by making use of the Eems flood barrier to influence the tidal currents. This could have a serious impact since the behaviour of water dynamics in the estuary is dominated by these tidal currents. To this day this option is being investigated to decide whether experiments can be executed in 2022 regulating these currents. One idea is to close the flood barriers once a day, at high tide. Since less water comes into the estuary, one expects also less sludge enters the estuary.

## 1.2. Current research

Due to the importance of these areas and the proposed human interference in the landscape, various studies and research projects have been performed since the end of last century. A morphodynamic model of such a tidal embayment was first studied by Schuttelaars & de Swart (1996). They did analytical research on an idealized embayment with stratified boundaries, the bottom elevation changing over space, as well as in time due to sedimentation processes. At a certain moment in this thesis the seabed is considered to be constant. However, in contrast to Schuttelaars & de Swart (1996), the side boundaries can vary over the length of the embayment. The situation without externally prescribed overtide is considered.

The embayment is idealized using various assumptions and simplifications, the water motion is described by the Shallow Water Equations (Vreugdenhil, 1994). The model domain is width and depth averaged. This gives a cross-sectional averaged set of equations, i.e. a one-dimensional system. The resulting water motion is obtained analytical and interpreted (Friederichs & Madsen, 1992). In this work, the boundaries at the sides of the estuary are supposed to have zero depth, where in this thesis the water depth is the same everywhere, including at the boundaries, i.e. the water depth does not vanish at the boundaries. One part somewhat arbitrary in the middle of the basin can be narrowed or widened over time. Goal is to simulate a flood barrier which can be partly closed.

Figure 1.3: The Eems flood barrier. Upstream in the German industries, cruise ships are assembled and transferred via this barrier.

The crux lies in the fact that the barrier cross-section can be altered in time. Due to this temporally varying barrier, the equations are not analytically solvable and a numerical solution procedure has to be followed.

Since it is not possible to check these solutions against ones analytical obtained in the complex case, there will be a comparison with solutions from analytical results, when the width is not varying in

time.

**Research questions** The main goal of this thesis is to investigate tidal properties of two basins connected with a time dependent horizontal moving barrier. The barrier will move periodic in time. This will influence the sedimentation in the estuary, which leads to the following research question:

> Q1: How does a periodic movable barrier influence the currents and water levels in an estuary driven by tidal forcing?
>
> Q2: Are there manipulations to the barrier that suffices to minimize the sedimentation in the estuary?

How do all the currents and water levels affect the sediment transport in the estuary? The current velocity $u$ acts as a proxy for the sediment transport $q$; more specifically $\langle q \rangle$ is modeled as being proportional to $\langle u^3 \rangle$. So if the velocity is obtained at every point in the basin at all times, the sediment transport can be plotted. Is it possible to determine the estuarine turbidity maxima for various phase shifts in the border prescription? And to what extent can possible solutions be given to remedy these phenomena? This thesis does not strive to give quantitative answers nor hard numbers, but opts to give insight into the behaviour of the currents and point out the possibilities for further investigation.

## 1.3. Thesis structure

The organization of this thesis is as follows. In chapter 2 the equations used to model the water motions will be given. The assumptions made are explained. Chapter 3 introduces the numerical approach used to solve the one dimensional shallow water equations. In chapter 4 the results are presented. In chapter 5 the results are elaborated and a final conclusion is drawn.

# 2

# Derivation of the one dimensional Shallow Water Equations

In this chapter a cross-sectional model is derived to describe the tidal dynamics in an estuary. First the geometry of the basin is presented and idealisations are discussed. Next, the conservation of mass and momentum are presented. These three dimensional equations are integrated first over the depth and finally over the width, resulting in a cross-sectionally averaged model. Subtleties in the cross-sectional derivations will be important throughout the research, so this section is elaborated in more detail.

## 2.1. Geometry

A top view and side view of an estuary that will be used in the remainder of this thesis is schematically displayed in figure (2.1). The length of the estuary is denoted by a constant length *L*, the depth *H*

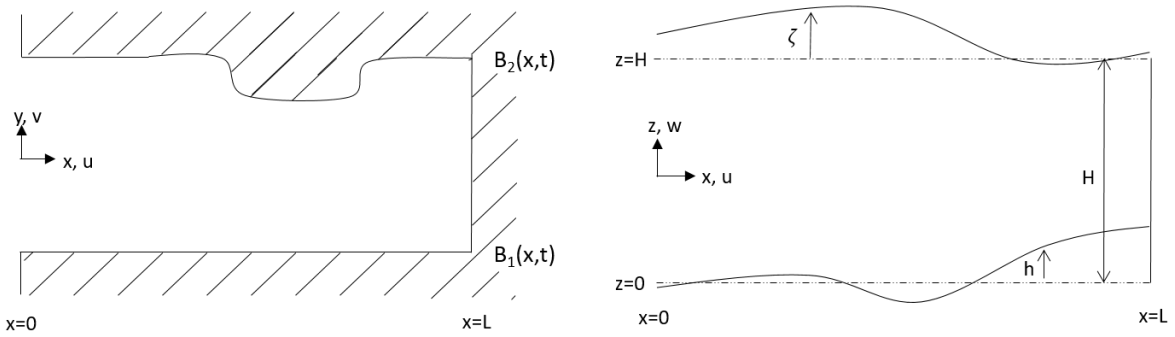


Figure 2.1: The geometry of the estuary is schematically displayed. In the left panel the top view is given. The border is able to vary temporally and spatially. The right panel denotes a side view of the estuary, where the bottom elevation can alter, denoted with *h*. The surface elevation is given by $\zeta$.

denotes the water depth at the entrance of the estuary, while deviations from the depth are indicated by *h*. The coordinate system is chosen such that the connection to the open sea is found at $x = 0$ and the landward end is found at $x = L$. The depth of the estuary is considered to be much smaller than the length and width of the basin. The non-erodible side walls are located at $B_1$ and $B_2$. For the Coriolis force it is important to take the x-, y-, and z-direction respectively east-, north-, and upward. The water velocity in the x-, y-, and z-direction is denoted by *u*, *v* and *w* respectively. The side borders are able to vary temporally and spatially.

## 2.2. Model Formulation

Given the three dimensional Navier Stokes equation, goal is to arrive at a certain simplicity, where it is possible to solve the set of equations analytically or approach them numerical. Simplifications are obtained using various assumptions.

### 2.2.1. 3 dimensional unsteady Navier Stokes

The equations modeling the water motion in an incompressible medium are given by

$$\frac{\partial u}{\partial x} + \frac{\partial v}{\partial y} + \frac{\partial w}{\partial z} = 0, \tag{2.1a}$$

$$\frac{\partial u}{\partial t} + u\frac{\partial u}{\partial x} + v\frac{\partial u}{\partial y} + w\frac{\partial u}{\partial z} + f_* w - fv = -\frac{1}{\rho}\frac{\partial p}{\partial x} + \nu\left(\frac{\partial^2 u}{\partial x^2} + \frac{\partial^2 u}{\partial y^2} + \frac{\partial^2 u}{\partial z^2}\right), \tag{2.1b}$$

$$\frac{\partial v}{\partial t} + u\frac{\partial v}{\partial x} + v\frac{\partial v}{\partial y} + w\frac{\partial v}{\partial z} + fu = -\frac{1}{\rho}\frac{\partial p}{\partial y} + \nu\left(\frac{\partial^2 v}{\partial x^2} + \frac{\partial^2 v}{\partial y^2} + \frac{\partial^2 v}{\partial z^2}\right), \tag{2.1c}$$

$$\frac{\partial w}{\partial t} + u\frac{\partial w}{\partial x} + v\frac{\partial w}{\partial y} + w\frac{\partial w}{\partial z} - f_* u = -\frac{1}{\rho}\frac{\partial p}{\partial z} + \nu\left(\frac{\partial^2 w}{\partial x^2} + \frac{\partial^2 w}{\partial y^2} + \frac{\partial^2 w}{\partial z^2}\right) - g, \tag{2.1d}$$

where 2.1a models the continuity of mass, while (2.1b) - (2.1d) are the momentum equations in the *x*, *y* and *z* direction respectively. In these equations, $t$ is the variable for time, $\rho$ denotes the density of the water. The Coriolis parameter and the reciprocal Coriolis parameter are given by *f* and $f_*$, respectively. $\nu$ indicates the kinematic viscosity, *p* is the pressure and *g* is the gravitational acceleration. The system of equations (2.1) resolves the turbulent length- and timescales. To focus on larger scales, which are of interest for the tidal motion, the so-called Reynolds decomposition is used (Pedlosky, 1987):

$$u = \langle u \rangle + u', \tag{2.2}$$

with $\langle u \rangle$ the ensemble averaged qualities, and $u'$ deviations from the average. Omitting a full derivation, the Reynolds averaged equations are obtained, in which the brackets are omitted for readability:

$$\frac{\partial u}{\partial x} + \frac{\partial v}{\partial y} + \frac{\partial w}{\partial z} = 0, \tag{2.3a}$$

$$\frac{\partial u}{\partial t} + u\frac{\partial u}{\partial x} + v\frac{\partial u}{\partial y} + w\frac{\partial u}{\partial z} + f_* w - fv = -\frac{1}{\rho}\frac{\partial p}{\partial x} + \frac{\partial}{\partial x}\left(\mathcal{A}_h\frac{\partial u}{\partial x}\right) + \frac{\partial}{\partial y}\left(\mathcal{A}_h\frac{\partial u}{\partial y}\right) + \frac{\partial}{\partial z}\left(\mathcal{A}_v\frac{\partial u}{\partial z}\right), \tag{2.3b}$$

$$\frac{\partial v}{\partial t} + u\frac{\partial v}{\partial x} + v\frac{\partial v}{\partial y} + w\frac{\partial v}{\partial z} + fu = -\frac{1}{\rho}\frac{\partial p}{\partial y} + \frac{\partial}{\partial x}\left(\mathcal{A}_h\frac{\partial v}{\partial x}\right) + \frac{\partial}{\partial y}\left(\mathcal{A}_h\frac{\partial v}{\partial y}\right) + \frac{\partial}{\partial z}\left(\mathcal{A}_v\frac{\partial v}{\partial z}\right), \tag{2.3c}$$

$$\frac{\partial w}{\partial t} + u\frac{\partial w}{\partial x} + v\frac{\partial w}{\partial y} + w\frac{\partial w}{\partial z} - f_* u = -\frac{1}{\rho}\frac{\partial p}{\partial z} + \frac{\partial}{\partial x}\left(\mathcal{A}_h\frac{\partial w}{\partial x}\right) + \frac{\partial}{\partial y}\left(\mathcal{A}_h\frac{\partial w}{\partial y}\right) + \frac{\partial}{\partial z}\left(\mathcal{A}_v\frac{\partial w}{\partial z}\right) - g, \tag{2.3d}$$

where the horizontal and vertical eddy viscosities are introduced, denoted by $\mathcal{A}_h$ and $\mathcal{A}_v$. These equations are valid for a wide range of problems. To further simplify, the equations are made dimensionless. This will allow the simplification of equations (2.3) to the so-called Shallow Water Equations. For the case considered, the length of the basin (order of kilometers) is much larger than the depth (order of meters). The horizontal and vertical length scales are denoted by *L* and *H* respectively with $H << L$. Typical horizontal and vertical flows are denoted by *U* and *W*. This results in a scaling of equation (2.1a), given by

$$\frac{\partial u}{\partial x} + \frac{\partial v}{\partial y} + \frac{\partial w}{\partial z} = 0. \tag{2.4}$$

$$\frac{U}{L} \qquad \frac{U}{L} \qquad \frac{W}{H}$$

This results in $\frac{U}{L} \sim \frac{W}{H}$, since they have to balance each other out. Making use of the fact that the Length *L* is way larger than *H* results in $H/L << 1$. Substituting this fact in above equation yields $W << U$. Thus it can be concluded here, regarding shallow water, that the flow is mainly horizontal. When this outcome is considered in cooperation with a dimensional check of the momentum equation in the vertical direction stated in equation (2.3d), one arrives at the hydrostatic balance, in accordance to (Pedlosky, 1987):

$$\frac{\partial p}{\partial z} = -\rho g. \tag{2.5}$$

Furthermore, using dimensionless analysis, the reciprocal Coriolis terms can be neglected in the horizontal momentum equations (2.3b) and (2.3c) (Cushman-Roisin and Beckers, 2009). All of this com-

bined results in the hydrostatic shallow water equations, fully describing the system as

$$\frac{\partial u}{\partial x} + \frac{\partial v}{\partial y} + \frac{\partial w}{\partial z} = 0, \tag{2.6a}$$

$$\frac{\partial u}{\partial t} + u\frac{\partial u}{\partial x} + v\frac{\partial u}{\partial y} + w\frac{\partial u}{\partial z} - fv = -\frac{1}{\rho}\frac{\partial p}{\partial x} + \frac{\partial}{\partial x}(\mathcal{A}_h\frac{\partial u}{\partial x}) + \frac{\partial}{\partial y}(\mathcal{A}_h\frac{\partial u}{\partial y}) + \frac{\partial}{\partial z}(\mathcal{A}_v\frac{\partial u}{\partial z}), \tag{2.6b}$$

$$\frac{\partial v}{\partial t} + u\frac{\partial v}{\partial x} + v\frac{\partial v}{\partial y} + w\frac{\partial v}{\partial z} + fu = -\frac{1}{\rho}\frac{\partial p}{\partial y} + \frac{\partial}{\partial x}(\mathcal{A}_h\frac{\partial v}{\partial x}) + \frac{\partial}{\partial y}(\mathcal{A}_h\frac{\partial v}{\partial y}) + \frac{\partial}{\partial z}(\mathcal{A}_v\frac{\partial v}{\partial z}), \tag{2.6c}$$

$$\frac{\partial p}{\partial z} = -\rho g. \tag{2.6d}$$

In equation (2.6b) the eddy viscosities can be replaced by the following equation:

$$\frac{\tau_{bx}}{\rho} = -\mathcal{A}_h\frac{\partial u}{\partial x}\frac{\partial h}{\partial x} - \mathcal{A}_h\frac{\partial u}{\partial y}\frac{\partial h}{\partial y} + \mathcal{A}_v\frac{\partial u}{\partial z}. \tag{2.7}$$

This too holds for $\tau_{by}$ in equation (2.6c), when the variable *x* is changed into the *y*-direction. To solve for the water motion, boundary conditions have to be imposed. Focusing on the vertical segment, there are two kinds: the kinematic and the dynamic boundary conditions.

**Kinematic boundary conditions** This condition states that a free particle of the water on the surface stays on the surface. The free surface is given by

$$z_p = H + \zeta(x_p, y_p, t).$$

Taking the total time derivative of this expressions results in

$$w = \frac{\partial \zeta}{\partial t} + u\frac{\partial \zeta}{\partial x} + v\frac{\partial \zeta}{\partial y}, \tag{2.8}$$

which states the kinematic boundary condition at the surface. Likewise, a similar condition can be derived at the bottom ($z = h$):

$$w = \frac{\partial h}{\partial t} + u\frac{\partial h}{\partial x} + v\frac{\partial h}{\partial y}. \tag{2.9}$$

**Dynamic boundary conditions** The dynamic boundary at the sea surface and the bottom is necessary to provide the conditions for the tangential stresses.

Through both empirical and dimensional analysis it is obtained that the bottom shear-stress is quadratic in the local tangential velocity (de Swart, 2009; Burchard et al., 2011), resulting in the quadratic bottom stress law:

$$\frac{\tau_{bx}}{\rho} = C_d\sqrt{u_b^2 + v_b^2}u_b, \tag{2.10}$$

with the drag coefficient defined as $C_d$; $u_b$ and $v_b$ denote the horizontal velocities at the bottom in the x- and y-direction respectively. This relation is nonlinear. Fortunately, Lorentz showed that when this system is forced by a dominant frequency, this relation can be linearised (de Swart, 2009; Vreugdenhil, 1994), resulting in

$$\frac{\tau_{bx}}{\rho} = ru_b.$$

A similar approach is taken for the *y*-direction.

The surface shear stress can be related in the shear stress executed by the wind. This is the stress that acts from the air directly onto the sea surface. This effect is often parameterised using the wind speed at 10 meters above surface:

$$\frac{\tau_{wx}}{\rho} = \frac{\rho_a}{\rho}C_d\sqrt{u_{10}^2 + v_{10}^2}u_{10}$$

In this research, however, wind effects will be neglected.

### 2.2.2. Depth-averaged horizontal Shallow Water Equations

In this section a depth averaged model is obtained of the tidal dynamics in an estuary. The geometry of the basin is stated and explained; certain properties of the estuary are idealised and simplified. The conservation of mass and conservation of momentum are presented in next section, to arrive at a depth averaged two dimensional model. In this section the two dimensional shallow water equations will be derived. Since the depth dependent velocities will not play a significant role in this research, the subtleties of the derivations will be stated in the appendix. The mayor assumptions, as well as the necessary information and conditions will be discussed from below.

**Depth averaged conservation of mass** To arrive at the depth averaged conservation of mass, the three dimensional continuity equation (2.6a) is taken as starting point:

$$\frac{\partial u}{\partial x} + \frac{\partial v}{\partial y} + \frac{\partial w}{\partial z} = 0.$$

The most important tool is the use of Leibniz's integral rule, as stated in appendix A.1. To omit a lengthy and possibly confusing thesis the full derivation is put down in the appendix. Necessary for the understanding of the depth averaged equations, are the depth average velocities, defined as

$$\overline{u} = \frac{1}{H+\zeta-h}\int_h^{H+\zeta} u dz, \tag{2.11a}$$

$$\overline{v} = \frac{1}{H+\zeta-h}\int_h^{H+\zeta} v dz. \tag{2.11b}$$

Using the kinematic boundary conditions and the depth averaged velocities provides the depth-averaged continuity equation:

$$\frac{\partial \zeta}{\partial t} - \frac{\partial h}{\partial t} + \frac{\partial}{\partial x}[(H+\zeta-h)\overline{u}] + \frac{\partial}{\partial y}[(H+\zeta-h)\overline{v}] = 0. \tag{2.12}$$

**Depth averaged conservation of momentum** Similarly, the horizontal momentum equation (2.6b) is integrated over depth, resulting in (see Appendix A) the depth averaged conservation of momentum:

$$\frac{\partial \overline{u}}{\partial t} + \overline{u}\frac{\partial \overline{u}}{\partial x} + \overline{v}\frac{\partial \overline{u}}{\partial y} - f\overline{v} = -g\frac{\partial \zeta}{\partial x} + \frac{1}{H+\zeta-h}(-r\overline{u} + \frac{\partial}{\partial x}\mathcal{A}_h(H+\zeta-h)\frac{\partial \overline{u}}{\partial x}) + \frac{\partial}{\partial y}(\mathcal{A}_h(H+\zeta-h)\frac{\partial \overline{u}}{\partial x}).$$

By scaling the momentum equation, the order of magnitude of the various terms can be assessed. Again *u* is scaled with *U*; *L* and *H* are also taken into account in this section. The water motion at the inlet is forced with a $M_2$ tide, i.e. a semidiurnal tidal constituent with amplitude *A* and angular frequency $\sigma$. Finally, the dispersion relation for shallow water is needed, denoted by $\lambda = \sqrt{gH}/\sigma$. This all in cooperation with equation (2.6a) gives

$$\sigma A = \frac{HU}{L},$$

resulting in a typical scale for *U*. This results in the following scales for the various terms:

$$\frac{\partial \overline{u}}{\partial t} + \overline{u}\frac{\partial \overline{u}}{\partial x} + \overline{v}\frac{\partial \overline{u}}{\partial y} - f\overline{v} = -g\frac{\partial \zeta}{\partial x} + \frac{1}{H+\zeta-h}(-r\overline{u} + \frac{\partial}{\partial x}\mathcal{A}_h(H+\zeta-h)\frac{\partial \overline{u}}{\partial x}) + \frac{\partial}{\partial y}(\mathcal{A}_h(H+\zeta-h)\frac{\partial \overline{u}}{\partial x})$$

$$\begin{array}{cccccccc} 1 & \frac{U}{\sigma L} & \frac{U}{\sigma L} & \frac{f}{\sigma} & \frac{\lambda^2}{L^2} & \frac{r}{\sigma H} & \frac{\mathcal{A}_h}{\sigma L^2} & \frac{\mathcal{A}_h}{\sigma L^2}, \\ 1 & 0.07 & 0.07 & 0.7 & 16 & 0.2 & 0.0002 & 0.0002 \end{array}$$

where the typical numbers are taken in line with Schuttelaars & de Swart (1996). It becomes clear that the horizontal eddy viscosity does not play a significant role and will thus be neglected in the remainder. Noteworthy is that these assumptions are made for the inner part of the basin. Very close

to the boundaries other length scales may dominate, resulting in another balance. However, since the focus is on the inner part of the basin, the depth averaged momentum equations read

$$\frac{\partial \overline{u}}{\partial t} + \overline{u}\frac{\partial \overline{u}}{\partial x} + \overline{v}\frac{\partial \overline{u}}{\partial y} - f\overline{u} = -g\frac{\partial \zeta}{\partial x} - \frac{r\overline{u}}{H+\zeta-h}, \tag{2.13a}$$

$$\frac{\partial \overline{v}}{\partial t} + \overline{u}\frac{\partial \overline{v}}{\partial x} + \overline{v}\frac{\partial \overline{v}}{\partial y} + f\overline{v} = -g\frac{\partial \zeta}{\partial y} - \frac{r\overline{v}}{H+\zeta-h}. \tag{2.13b}$$

Together with equation (2.12) these equations constitute the two dimensional horizontal Shallow Water Equations.

### 2.2.3. Cross-sectionally averaged Shallow Water Equations

In this section the one dimensional shallow water equations will be derived. Subtleties in the derivations will be important throughout the research. For this reason every mayor step is taken into account and treated.

**Boundary conditions** No water can flow through a solid impermeable wall. Mathematically this implies that a particle at the boundary stays at the boundary. Denoting the boundary by $B_n(t)$ for $n = 1, 2$, this condition requires that $\frac{dy}{dt} = \frac{dB_n}{dt}$; i.e.

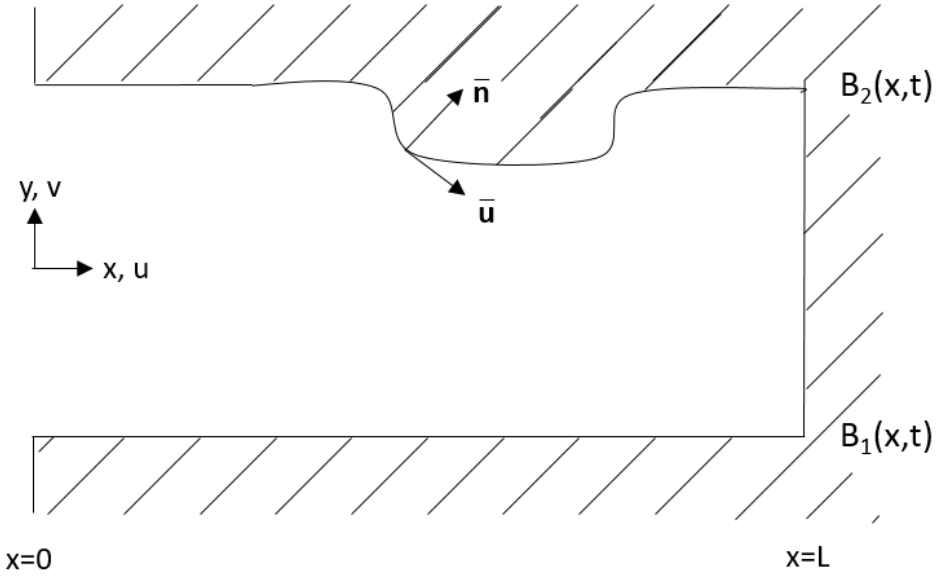


Figure 2.2: Geometry of an estuary. The side borders are considered to be time dependent and the width is variable over the length of the embayment. The direction of the normal vector **n** and current vector **u** are shown. The open connection to the sea lies at $x = 0$.

$$v = \frac{\partial B_n}{\partial t} + u\frac{\partial B_n}{\partial x}.$$

Note that if the boundary $B_n$ is fixed in time, this condition reduces to the condition of no transport through the boundary; $\vec{u} \cdot \vec{n} = 0$, where $\vec{n}$ denotes the normal vector. This means that at $B_1(x,t)$ and $B_2(x,t)$ there is no net water flow through the wall. This provides the boundary condition at the lower boundary $B_1(x,t)$ and upper boundary $B_2(x,t)$ respectively:

$$\frac{\partial B_1}{dt} + \overline{u}\frac{\partial B_1}{\partial x} - \overline{v} = 0, \tag{2.14a}$$

$$-\frac{\partial B_2}{dt} - \overline{u}\frac{\partial B_2}{\partial x} + \overline{v} = 0. \tag{2.14b}$$

**Width & depth averaged conservation of mass B(x,t)** The depth averaged conservation of mass is already obtained. To acquire the width average, this equation has to be integrated over the width; more specifically from $B_1(x,t)$ to $B_2(x,t)$:

$$\int_{B1}^{B2}[\frac{\partial \zeta}{\partial t} - \frac{\partial h}{\partial t} + \frac{\partial}{\partial x}((H+\zeta-h)\overline{u}) + \frac{\partial}{\partial y}((H+\zeta-h)\overline{v})]dy = 0,$$

or

$$\int_{B1}^{B2}[\frac{\partial}{\partial t}(H+\zeta-h) + \frac{\partial}{\partial x}((H+\zeta-h)\overline{u}) + \frac{\partial}{\partial y}((H+\zeta-h)\overline{v})]dy = 0.$$

First, the width averages for the various physical qualities are defined. For $\psi = (\zeta, h, \overline{u}, \overline{v})$, it is defined as

$$\hat{\psi} = \frac{1}{B_2(x,t) - B_1(x,t)} \int_{B_1(x,t)}^{B_2(x,t)} \psi dy.$$

Using the boundary conditions, the following result is obtained (together with Leibniz's integral rule and the fundamental theorem of calculus):

$$\frac{\partial}{\partial t}(\int_{B_1(x,t)}^{B_2(x,t)}(H+\zeta-h)dy) + \frac{\partial}{\partial x}(\int_{B_1(x,t)}^{B_2(x,t)}(H+\zeta-h)\overline{u}dy)$$
$$+((H+\zeta-h)(\frac{\partial B_1(x,t)}{\partial t} + \overline{u}\frac{\partial B_1(x,t)}{\partial x} - \overline{v}))_{B_1(x,t)} - ((H+\zeta-h)(\frac{\partial B_2(x,t)}{\partial t} + \overline{u}\frac{\partial B_2(x,t)}{\partial x} - \overline{v}))_{B_2(x,t)} = 0, \tag{2.15}$$

where both $B_1$ and $B_2$ are allowed to vary in time. The last two terms vanish due to the imposed boundary conditions in 2.14, resulting in

$$\frac{\partial}{\partial t}\{\int_{B_1(x,t)}^{B_2(x,t)}(H+\zeta-h)dy\} + \frac{\partial}{\partial x}(\int_{B_1(x,t)}^{B_2(x,t)}(H+\zeta-h)\overline{u}dy) = 0.$$

Each physical variable can be written in terms of is width mean and fluctuating parts. For $\zeta$, $h$ and $\overline{u}$ this is $\zeta = \hat{\zeta} + \tilde{\zeta}$, $h = \hat{h} + \tilde{h}$ and $\overline{u} = \hat{\overline{u}} + \tilde{\overline{u}}$ respectively. The fluctuating part has the property that the width average zero is:

$$\int_{B_1(x,t)}^{B_2(x,t)} \tilde{\zeta} dy = 0.$$

Using this notation, the product of two physical quantities, integrated over the width gives a part in terms of the product of the mean and a covariance term, for example

$$\int_{B_1}^{B_2}(H+\zeta-h)\overline{u}dy = (B_2-B_1)(H+\hat{\zeta}-\hat{h})\hat{\overline{u}} + \int_{B_1}^{B_2}(\tilde{\zeta}-\tilde{h})\tilde{\overline{u}}dy.$$

Neglecting the covariance variables, the following equation is obtained:

$$\frac{\partial}{\partial t}[((B_2-B_1)(H+\hat{\zeta}-\hat{h})] + \frac{\partial}{\partial x}(((B_2-B_1)(H+\hat{\zeta}-\hat{h})\hat{\overline{u}}) = 0. \tag{2.16}$$

If the width of the basin is considered to be constant in space and time, the equation can be further simplified to

$$\frac{\partial}{\partial t}(H+\hat{\zeta}-\hat{h}) + \frac{\partial}{\partial x}((H+\hat{\zeta}-\hat{h})\hat{\overline{u}}) = 0. \tag{2.17}$$

If the depth is assumed to vanish at the sides, expression 2.16 reduces to

$$(B_2(x)-B_1(x))\frac{\partial}{\partial t}(H+\hat{\zeta}-\hat{h}) + \frac{\partial}{\partial x}[(B_2(x)-B_1(x))(H+\hat{\zeta}-\hat{h})\hat{\overline{u}}] = 0$$

This expression is the one derived in Friedrichs & Madsen (1992).

If the depth at the time dependent boundary does not vanish, using $B = B_2(x,t)$ and taking $B_1(x,t) = 0$, and assuming that the depth and water deviation $\zeta$ is constant over the width, the cross-sectionally averaged conservation equation of mass is found. It reads

$$B\frac{\partial}{\partial t}(H + \hat{\zeta} - \hat{h}) + \frac{\partial}{\partial x}((H + \hat{\zeta} - \hat{h})B\hat{\overline{u}}) + [H + \hat{\zeta} - \hat{h}]_B \frac{\partial B}{\partial t} = 0. \tag{2.18}$$

**Width & depth averaged conservation of momentum** Just like the conservation of mass, the depth averaged conservation of momentum is already obtained. To acquire the width average, various assumptions and observations are made. The viscous terms were already shown to be small. Furthermore, considering a narrow basin compared to the Rossby deformation radius length scale, the Coriolis forces can be neglected (Schuttelaars & de Swart, 1990). The momentum equation for depth average in conservative form reads

$$\frac{\partial}{\partial t}((H + \zeta - h)\overline{u}) + \frac{\partial}{\partial x}((H + \zeta - h)\overline{u}^2) + \frac{\partial}{\partial y}((H + \zeta - h)\overline{uv})$$

$$= -(H + \zeta - h)g\frac{\partial \zeta}{\partial x} + r\overline{u}. \tag{2.19}$$

Similar to the derivation of the width averaged continuity equation, this equation is integrated over the width (using the boundary conditions), resulting in

$$\frac{\partial \hat{\overline{u}}}{\partial t} + \hat{\overline{u}}\frac{\partial \hat{\overline{u}}}{\partial x} = -g\frac{\partial \hat{\zeta}}{\partial x} - \frac{r\hat{\overline{u}}}{H + \hat{\zeta} - \hat{h}}. \tag{2.20}$$

Together with equation (2.18) these two equations form the cross-sectionally averaged shallow water equations.

## 2.2.4. Scaling of the equation

By making the equations dimensionless, it is possible to see which terms are dominant in the cross-sectional averaged equations. To simplify notation, hats and overbars denoting the depth and width averaging will be omitted from now on, hence all qualities are cross-sectionally averaged. To that end, the variables are made dimensionless as

$$x = Lx^*, \quad h = Hh^*, \quad u = Uu^*, \quad B = \beta B^*,$$

$$t = \frac{1}{\sigma}t^*, \quad \zeta = \frac{HU}{\sigma L}\zeta^* = A\zeta^*, \tag{2.21}$$

Where the scaling term for the deviation $\zeta$ follows from the balance between the first and last term in the conservation of mass, where *A* denotes the typical tidal amplitude. Substituting this in the one dimensional equations, one finds for the continuity equation that

$$\beta\sigma H\frac{\partial}{\partial t^*}[B^*(1 + \frac{U}{\sigma L}\zeta^* - h^*)] + \beta\frac{HU}{L}\frac{\partial}{\partial x^*}[(1 + \frac{U}{\sigma L}\zeta^* - h^*)u^*B^*] = 0.$$

By defining $\epsilon = \frac{HU}{\sigma L} = \frac{A}{H}$ and dividing by $\frac{HU}{L}$, this equation can be written to

$$\frac{\partial}{\partial t^*}[B^*(\frac{1}{\epsilon} + \zeta^* - \frac{1}{\epsilon}h^*)] + \frac{\partial}{\partial x^*}[(1 + \epsilon\zeta^* - h^*)u^*B^*] = 0, \tag{2.22}$$

using a typical depth of $H = 10m$ and $A = 1m$, $\epsilon \sim 0.1$ (Schuttelaars & de Swart, 1996). Furthermore, in this thesis the variable height *h* will be set to zero, resulting in

$$\frac{\partial}{\partial t^*}[B^*(\frac{1}{\epsilon} + \zeta^*)] + \frac{\partial}{\partial x^*}[(1 + \epsilon\zeta^*)u^*B^*] = 0$$

for the non-dimensional equation for conservation of mass.

**Conservation of momentum** In a similar manner the conservation of momentum can be made non-dimensional, resulting in

$$\sigma U\frac{\partial u^*}{\partial t^*}+\frac{U^2}{L}u^*\frac{\partial u^*}{\partial x^*}=-\frac{gHU}{\sigma L^2}\frac{\partial \zeta^*}{\partial x^*}-\frac{rU}{H}\frac{u^*}{1+\frac{u}{\sigma L}\zeta^*-h^*}.$$

Again, using the definition of $\epsilon$ and defining $\Lambda=\frac{gH}{\sigma^2L^2}$, one finds the non-dimensional balance as

$$\frac{\partial u^*}{\partial t^*}+\epsilon u^*\frac{\partial u^*}{\partial x^*}=-\Lambda\frac{\partial \zeta^*}{\partial x^*}-\frac{r}{\sigma H}\frac{u^*}{1+\epsilon\zeta^*-h^*}=0. \tag{2.23}$$

After using that $\epsilon << 1$ and recalling that $h=0$ once again, the non-dimensional leading order balance reads

$$\frac{\partial u^*}{\partial t^*}=-g\frac{\partial \zeta^*}{\partial x^*}-\frac{r}{\sigma H}u^*.$$

Since H is a constant, the latter term is rewritten by defining $\frac{r}{H}=\lambda$, which gives finally the linear momentum equation to be implemented and modeled:

$$\frac{\partial u}{\partial t}=-g\frac{\partial \zeta}{\partial x}-\lambda u, \tag{2.24a}$$

$$\frac{\partial}{\partial t}[(H+\zeta)B]+H\frac{\partial}{\partial x}[Bu]=0, \tag{2.24b}$$

where the non-dimensional quantities have been replaced with their dimensional variables as defined in equations (2.2.4).

# 3

# Solution method

## 3.1. Set of equations and boundary conditions

The system obtained in previous chapter, which has to be solved is given by

$$\frac{\partial u}{\partial t} = -g\frac{\partial \zeta}{\partial x} - \lambda u,$$

$$\frac{\partial}{\partial t}[(H+\zeta)B] + H\frac{\partial}{\partial x}[Bu] = 0,$$

where $B$, $u$ and $\zeta$ are both temporally and spatially variable quantities. This one dimensional system of equations has two imposed boundary conditions:

$$\zeta(0,t) = \hat{Z}cos(\sigma t), \tag{3.1a}$$

$$u(L,t) = 0, \tag{3.1b}$$

where $\hat{Z}$ denotes the amplitude of the tidal forcing at the inlet generated by the open sea. Furthermore, $\sigma$ describes the periodic frequency of the tidal forcing at $x = 0$. The latter boundary condition implies that water can not flow at the coastline ($x = L$), which results in a flow *u* that has to be zero at that point.

It is impossible to analytically solve the coupled set of equations (2.24). Therefore, a numerical procedure must be followed to solve this set. The equations are discretized and implemented in section 3.2. If the side boundaries are considered to be time independent, however, the equation in fact can be solved analytically; let alone if uniform boundaries are considered. Firstly, in upcoming section the time independent boundaries are solved. The resulting solutions can be compared to the numerical model. Negligible differences in the comparison give trust in the justification of using the same numerical procedure for the time dependent boundaries.

## 3.2. Analytical solutions

Considering the time independent boundaries, i.e. when the barrier does not vary in time, equations (2.24) reduce to

$$\frac{\partial u}{\partial t} = -g\frac{\partial \zeta}{\partial x} - \lambda u, \tag{3.2a}$$

$$B\frac{\partial \zeta}{\partial t} + H\frac{\partial}{\partial x}[Bu] = 0. \tag{3.2b}$$

To calculate the expressions for $\zeta$ and $u$, each equation is manipulated so it only depends on one of the two variables. First, the water level $\zeta$ is calculated. After this, $u$ is derived in a similar process. In order to obtain an expression for $\zeta(x,t)$ substitutions in equation (3.2a) are made, resulting in

$$B\frac{\partial^2 \zeta}{\partial t^2} + \lambda B\frac{\partial \zeta}{\partial t} - gH\frac{\partial}{\partial x}B(\frac{\partial \zeta}{\partial x}) = 0.$$

From this point, separation of variables is used. Suppose $\zeta = Re[Z(x)e^{-i\sigma t}]$. This assumption is justified due to the periodic forcing at the boundary (equation (3.1a)). Substituting in previous equation, applying the product rule and rewriting gives that

$$B(x)\frac{d^2Z(x)}{dx^2} + \frac{dB(x)}{dx}\frac{dZ(x)}{dx} + \frac{\sigma^2}{gH}(1 + i\frac{\lambda}{\sigma})B(x)Z(x) = 0. \tag{3.3}$$

The other earlier prescribed boundary condition (equation (3.1b)) valid too. In order to provide useful information, it is substituted at $x = L$ in equation (3.2a). This gives information regarding $\zeta$ at this position, making the second boundary condition to read as

$$\frac{\partial\zeta(L,t)}{\partial x} = 0.$$

From here it is possible to numerically approach this equation. To obtain the full expression for $\zeta(x,t)$, the solution for $Z(x)$ found in solving equation (3.3) has to be multiplied with its time dependent part $e^{-i\sigma t}$.

In a very similar way the water velocity $u(x,t)$ is analytically approached. Substituting and rewriting gives again an expression for $u$, which reads as

$$\frac{\partial^2 B(x)u}{\partial x^2} - \frac{1}{B(x)}\frac{\partial B(x)}{\partial x}\frac{\partial B(x)u}{\partial x} - \frac{B(x)}{gH}[\frac{\partial^2 u}{\partial t^2} + \frac{\lambda\partial u}{\partial t}] = 0.$$

Defining $u = Re[U(x)e^{-i\sigma t}]$ and dividing out the time dependent part results in

$$\frac{d^2B(x)U(x)}{dx^2} - \frac{1}{B(x)}\frac{dB(x)}{dx}\frac{dB(x)U(x)}{dx} + B(x)\frac{\sigma^2}{gH}(1 + i\frac{\lambda}{\sigma})U(x) = 0. \tag{3.4}$$

For the first boundary condition (equation (3.1a)) to be able to implement, it is substituted at $x = 0$. This provides information regarding $u$ at the inlet connected to the open sea:

$$B(0)[-i\sigma\hat{Z}e^{-i\sigma t}] + H(\frac{dB(0)U}{dx})e^{-i\sigma t} = 0.$$

The borders near $x = 0$ will not change. This means that $B(0)$ is constant, implying $\frac{dB(0)}{dx} = 0$. Dividing out the time dependent parts gives

$$B(0)[-i\sigma\hat{Z}] + HB(0)(\frac{dU}{dx}) = [-i\sigma\hat{Z}] + H(\frac{dU}{dx}) = 0,$$

Resulting in the boundary condition for $u$:

$$\frac{dU(0)}{dx} = \frac{i\sigma\hat{Z}}{H}$$

Similarly to the water level $\zeta$, it is possible to numerically approach this equation. To obtain the full expression for $u(x,t)$, the solution for $U(x)$ found in solving equation (3.4) has to be multiplied with its time dependent part $e^{-i\sigma t}$.

One special case worth considering is when the borders are uniform. $B(x,t)$ is constant and will thus vanish from equation (2.24b). The equations are solved, resulting in an expression for the water level and velocity as

$$\zeta(x,t) = Re\{\frac{\hat{Z}}{cos(k_*L)}cos[k_*(L-x)]e^{-i\sigma t}\}, \tag{3.5a}$$

$$u(x,t) = Re\{\frac{ig\hat{Z}}{c(1+i\hat{\lambda})^{\frac{1}{2}}}\frac{sin[k_*(L-x)]}{cos(k_*L)}e^{-i\sigma t}\}, \tag{3.5b}$$

where the variable $k_* = \frac{\sigma^2}{c^2}(1+i\frac{\lambda}{\sigma})$ is introduced for notation reasons; c denotes the wave speed, given by $c = \sqrt{gH}$ and $\hat{\lambda} = \frac{\lambda}{\sigma}$.

## 3.3. Numerical approach

The goal of this experiment is to investigate the impact of changes in the width of an estuary. Due to the time dependency of B(x,t), separation of variables is no longer an option. From here on it is only possible to use a numerical procedure to model the equations. Both the space and time directions have to be discretized. In order to obtain accurate solutions, a second order method is used. For time, a forward method will be employed. The total resulting method is called the Centred Space Forward Time method (CSFT).

To discretize the problem, the basin is divided in equally spaced discrete parts, labeled from $j = 0, 1, 2, ..., NX + 1$, each with a length of $\Delta x = \frac{L}{NX}$ meters. The time step $\Delta t$ is chosen somewhat arbitrarily, and is based on the stability conditions that will be discussed below. A total number of *NT* time steps is determined, with *NT* large enough to cover enough tidal cycles to perform the appropriate analysis. The time is indicated in a superscript $n$; the position in the estuary is labeled as a subscript $j$, i.e. the water velocity $u(j\Delta x, n\Delta t)$ is denoted by $u_j^n$. In this notation, $n$ indicates the time passed by $n\Delta t$ seconds, leading up to a maximum of $NT\Delta t$ seconds. The current evaluated position is situated at $j\Delta x$ meters inside the estuary. It was found that the most straightforward time stepping algorithm, the first order numerical approach (Euler forward), is unstable in all cases. The second order however is stable when it satisfies the Courant stability condition (Press, 1988), given by

$$c\frac{\Delta t}{\Delta x} \leq 1,$$

where *c* denotes the wave velocity $\sqrt{gH}$. In order to ensure stability, the Lax method is applied (Press, 1988; p.837), given by

$$u_j^n = \frac{1}{2}(u_{j+1}^n + u_{j-1}^n).$$

In this way the mean is taken at point $x = j\Delta x$ by averaging the values at $x = (j-1)\Delta x$ and $x = (j+1)\Delta x$. For the friction $\lambda$, an implicit scheme is chosen.

**Discretizing the time dependent width** The equations (2.24) can be rewritten to

$$\frac{\partial u}{\partial t} + g\frac{\partial \zeta}{\partial x} + \lambda u = 0, \tag{3.6a}$$

$$B(x,t)\frac{\partial \zeta}{\partial t} + H\frac{\partial B(x,t)u}{\partial x} + (H+\zeta)\frac{\partial B(x,t)}{\partial t} = 0, \tag{3.6b}$$

in order to ease the discretization. Using the information stated in the appendix, the discretization of above equations in a second order of convergence is given by

$$B_j^n\frac{\zeta_j^{n+1} - \zeta_j^n}{\Delta t} + H\frac{u_{j+1}^n B_{j+1}^n - u_{j-1}^n B_{j-1}^n}{2\Delta x} + (H + \zeta_j^n)\frac{B_j^{n+1} - B_j^n}{\Delta t} = 0, \tag{3.7a}$$

$$\frac{u_j^{n+1} - u_{j+1}^n}{\Delta t} + g\frac{\zeta_{j+1}^n - \zeta_{j-1}^n}{2\Delta x} + \lambda u_j^{n+1} = 0. \tag{3.7b}$$

Rewriting provides the explicit expressions for $\zeta$ and $u$, denoted by

$$\zeta_j^{n+1} = \frac{1}{2}\zeta_{j+1}^n + \frac{1}{2}\zeta_{j-1}^n - \frac{\Delta t}{2\Delta x}\frac{H}{B_j^n}[u_{j+1}^n B_{j+1}^n] + \frac{\Delta t}{2\Delta x}\frac{H}{B_j^n}[u_{j-1}^n B_{j-1}^n] - \zeta_j^n(\frac{B_j^{n+1}}{B_j^n} - 1) - H(\frac{B_j^{n+1}}{B_j^n} - 1), \tag{3.8a}$$

$$u_j^{n+1} = f\frac{1}{2}u_{j+1}^n + f\frac{1}{2}u_{j-1}^n - f\frac{\Delta t}{2\Delta x}g\zeta_{j+1}^n + f\frac{\Delta t}{2\Delta x}g\zeta_{j-1}^n, \tag{3.8b}$$

where $f = \frac{1}{1+\lambda\Delta t}$ is used to simplify the notation. Second order forward and backward derivatives are used to obtain discrete inward boundary conditions. With the other imposed boundary conditions (3.1),

this sums up to

$$\zeta_0^{n+1} = \hat{Z} cos(\sigma \Delta t(n+1)), \tag{3.9a}$$

$$u_0^{n+1} = f u_0^n + f \frac{3\Delta t}{2\Delta x} g \zeta_0^n - f \frac{4\Delta t}{2\Delta x} g \zeta_1^n + f \frac{\Delta t}{2\Delta x} g \zeta_2^n, \tag{3.9b}$$

$$\zeta_{nx}^{n+1} = \zeta_{nx}^n - \frac{3\Delta t}{2\Delta x} H u_{nx}^n + \frac{B_{nx-1}^n}{B_{nx}^n} \frac{4\Delta t}{2\Delta x} H u_{nx-1}^n - \frac{B_{nx-2}^n}{B_{nx}^n} \frac{\Delta t}{2\Delta x} H u_{nx-2}^n, \tag{3.9c}$$

$$u_{nx}^{n+1} = 0, \tag{3.9d}$$

obtaining together with equations (3.8) the entire system to be modeled. To validate this model, it is compared to the analytical solutions regarding the time independent and uniform boundaries. Many terms will score out, which means that the discretization can be drastically simplified. For this results in a shorter calculation time in the model, new discretizations are composed for these specific cases. Due to the shorter runtimes, the grid is made more detailed and will provide a better comparison. The full discretizations are displayed in the appendix.

# 4

# Results

## 4.1. Introduction

In this chapter the results, obtained with the cross-sectional set of equations, are elaborated. Firstly, the embayment with a constant width that does not change in time will be discussed. A snapshot of the current $u$ and water level $\zeta$ at high water and characteristic properties are discussed. Subsequently, the basin width is allowed to be non-uniform in space, though not yet variable in time. Again the water level and velocity are shown at high water. For both cases, the solutions are compared to the analytica solutions obtained with separation of variables. Finally the influence of a horizontally movable barrier, schematized as a time dependent width $B(x,t)$ is investigated. The influence of the periodically changing width on the water motion and the generation of overtides will be discussed. The consequences of these overtides on the sediment transport will be shown over the entire estuary, resulting in recommended possible solutions to the sludge problem.

## 4.2. Constant width B

In this section, the system of equations (2.24) will be solved for an estuary with a uniform, time-independent width. The solutions for the resulting system of equations can be obtained using both a numerical and an analytical approach. The width *B* is normalised and considered equal to 1 throughout the entire embayment. See fig (4.1) for a plan view of the geometry.

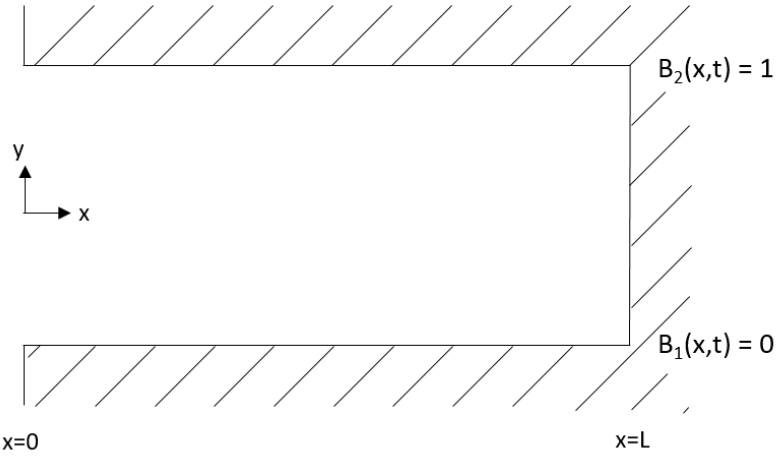


Figure 4.1: Schematic top view of a uniform estuary with normalised width. The side borders can not change in time, nor do they vary over the length of the estuary.

In fig (4.2), the water level variation $\zeta$ and velocity $u$ are shown at high water after 245 hours. The results were obtained using the numerical model, that was initiated with the analytical solutions at $t = 0$, i.e. after 20 tidal cycles the influence of initial condition is damped out and the final periodic

solution is found. The exact quantities used for the numerical procedure are shown in Appendix B.2. The results are compared with the analytical solution (shown in dashed lines). The difference between the numerical and analytical solution is very small, as showed in fig (4.3), giving trust in the numerical implementation of the solution procedure. One observes that the current is zero at the closed end ($x = L$). Furthermore, the water level is amplified at the coast, which is an indication that the basin is in resonance.

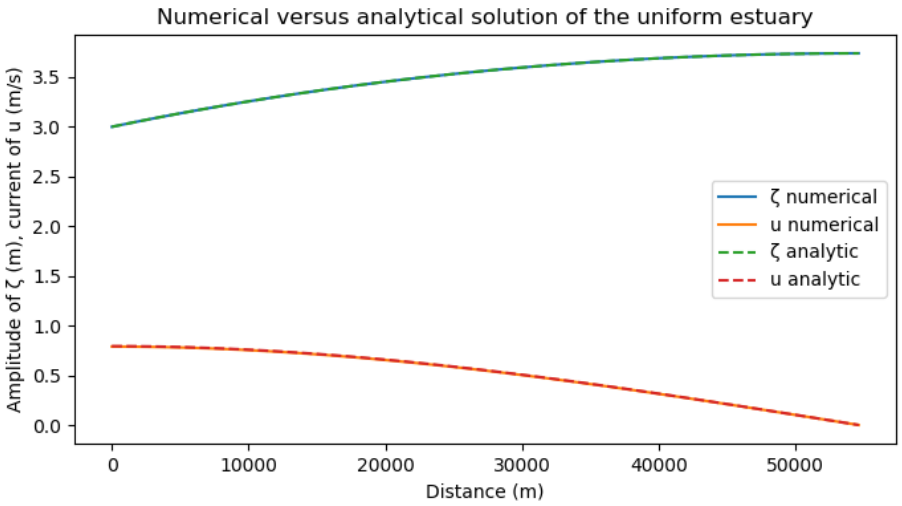


Figure 4.2: Solution in the uniform embayment after 245 hours. Analytical and numerical solutions are plotted with each other as a function of the position and time in the embayment.

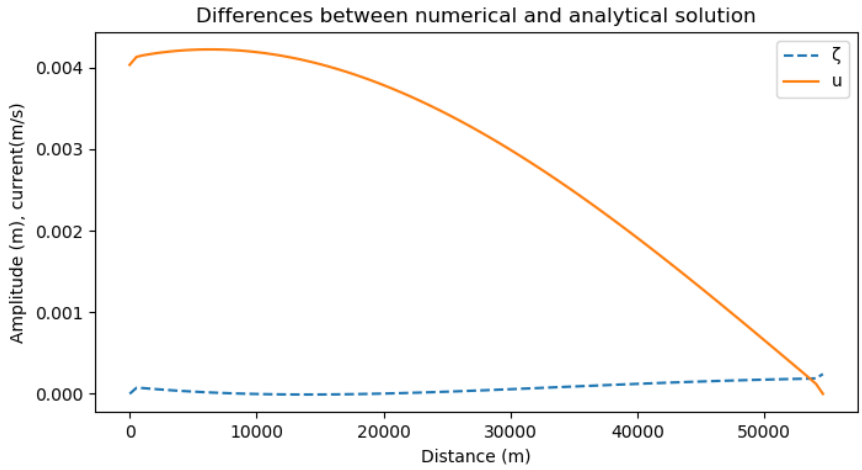


Figure 4.3: Differences of the solutions in a uniform embayment between the analytical and numerical method are plotted for the water motion: the difference in the water level $\zeta$ is denoted by a dashed line. The absolute difference in the velocity $u$ is given by the second line.

## 4.3. Spatial variation B(x)

In this section the width is allowed to vary over the length of the embayment. Here, focus lies on one particular situation, where the lower border $B_1(x)$ is considered to be constant and located at $y = 0$, while the top boundary is prescribed as:

$$B_2(x) = 1 - \frac{1}{4}tanh(\frac{(x - 30000)}{1000}) + \frac{1}{4}tanh(\frac{(x - 40000)}{1000}), \tag{4.1}$$

see fig (4.4). Again solid lines indicate the numerical approach, dashed lines display the analytic so-

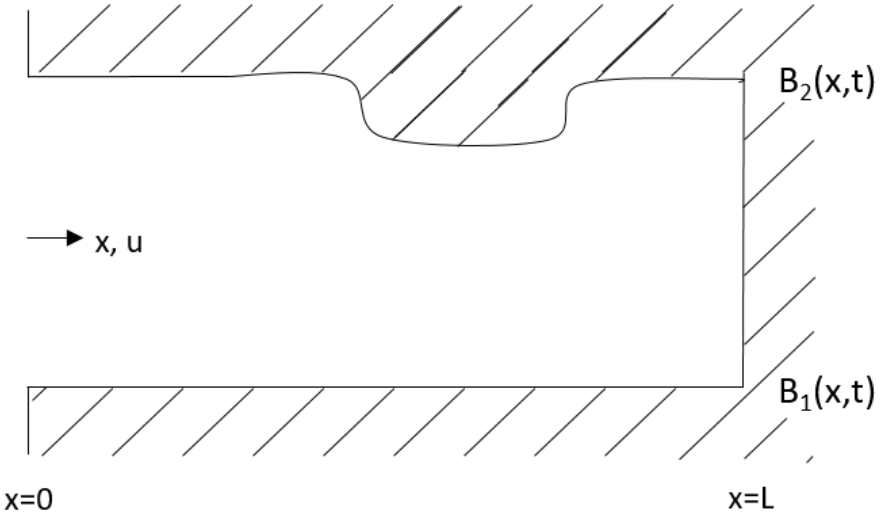


Figure 4.4: Geometry of the estuary with a narrowing barrier dependent on the position in the embayment. The first side border is set to be at $y = 0$. The second border varies accordingly to equation (4.1).

lution. No significant differences are seen between the numerical and the analytical solution. In figure (4.5) the water velocity *u* clearly shows an increase throughout the narrow part of the embayment. As soon as it widens (around 40 km) $u$ decreases again. This is in agreement with literature, which states that conservation of mass requires that *u* increases as *B* decreases (if frictional effects do not change), and vice versa. Furthermore, the solutions obtained in this section are plotted with the solutions found in the uniform embayment in order to compare the two, as shown in figure (4.6). The amplitude of the water level $\zeta$ is in the middle regions slightly lower than the solution considering the uniform estuary. The increasing current $u$ nearby the barrier, and higher value inside of the barrier is clearly visible. Passed the barrier, the water velocity tends towards the current of the uniform estuary. Near the inlet to the open sea, the water velocity is considerably smaller. It thus can be concluded that the influence of the barrier is present in the entire estuary; not only inside and near the barrier. One observes that the current is still zero at the closed end at x=L and the water level is still amplified at the coast.

The difference between the numerical and analytic solution is again small, as showed in fig (4.7),

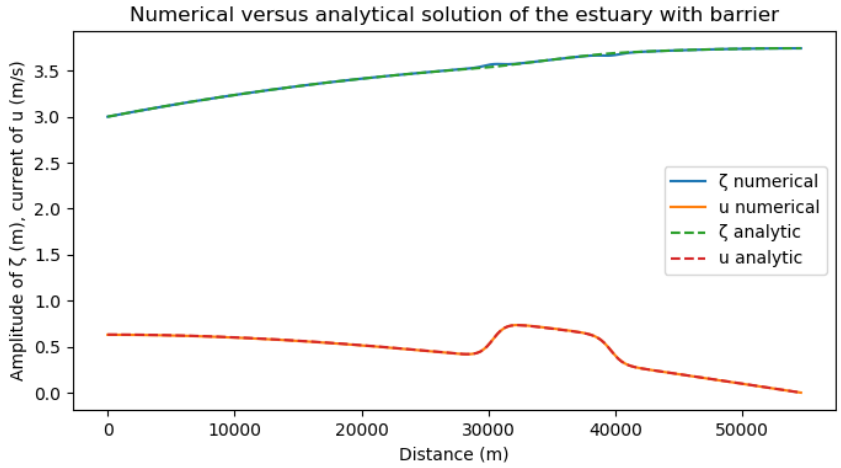


Figure 4.5: Solution in the estuary with the barrier (i.e. the narrowing embayment) measured after 245 hours. Analytical (dashed) and numerical solutions are plotted with each other.

giving trust in the numerical implementation of the solution procedure. As discussed in the previous chapter (see also the analytical solution), the solution is periodic because the forcing is a periodic func-

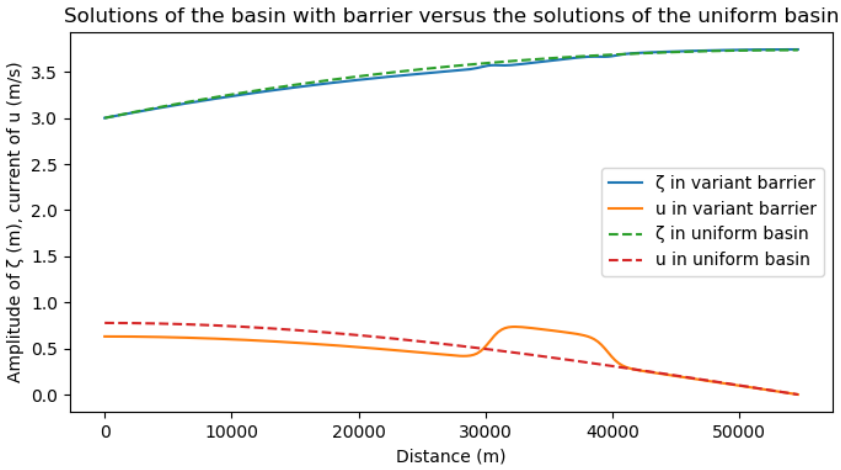


Figure 4.6: Solution in the estuary with the barrier (i.e. the narrowing embayment) measured after 245 hours plotted with the solution to the uniform estuary (dashed).

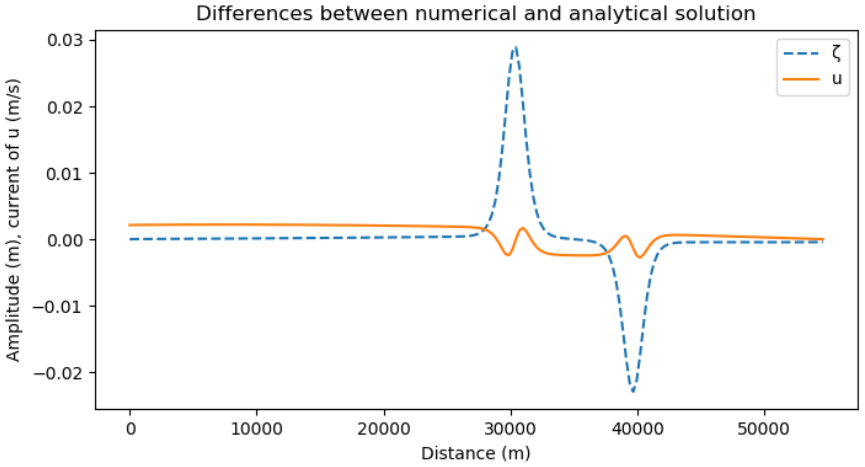


Figure 4.7: Differences of the solutions in the narrowing estuary between the analytical and numerical method are plotted for the water motion. The water level $\zeta$ is denoted by a dashed line, where the velocity $u$ is given by the second line.

tion. By using a fast Fourier transformation the periodicities in the water level and velocities can be identified.

In figure (4.8), left panel, the fast Fourier transform of the water level $\zeta$ is shown, and in the right panel the fast Fourier transform of the current velocity $u$ at a somewhat arbitrary point inside the narrow part in the barrier, namely at $x = 33km$. The signal has only one clear frequency, which is equal to the frequency of the periodic forcing. In fig (4.9) the phase and amplitude of both the water level and velocity in the estuary are displayed. The phase of $\zeta$ shows the lag of the tidal waves as the waves propagate through the estuary.

## 4.4. Width variations in both space and time B(x,t)

From here on separation of variables can not be performed anymore. Since the previous two cases show a good agreement between the analytical and the numerical solutions, the numerical code will be used to investigate the water motion where spatially and temporally varying width is allowed. The time variations of the width will be assumed to vary with the same frequency as the periodic forcing and is defined as

$$\mathcal{B}(x,t) = B(x)\{1 - cos(\sigma t - \phi)\}, \tag{4.2}$$

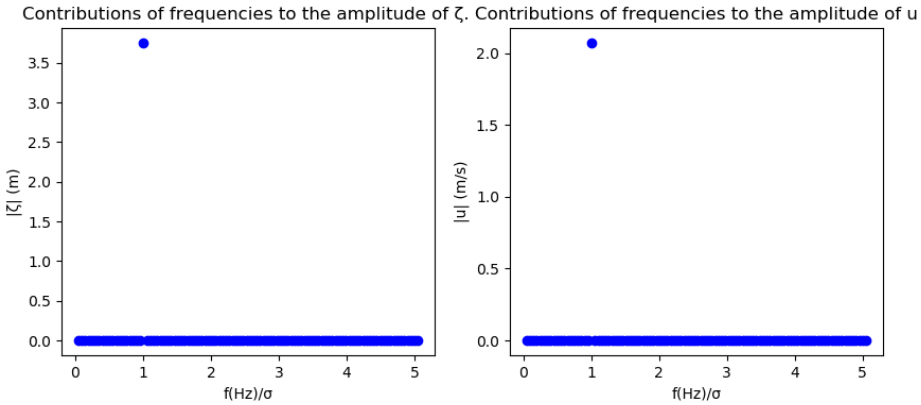


Figure 4.8: The absolute values of $\zeta$ (left) and $u$ (right) are displayed. It is a fft calculated at x=33km, so at the narrow part of the basin, taken over a time of ten periods.

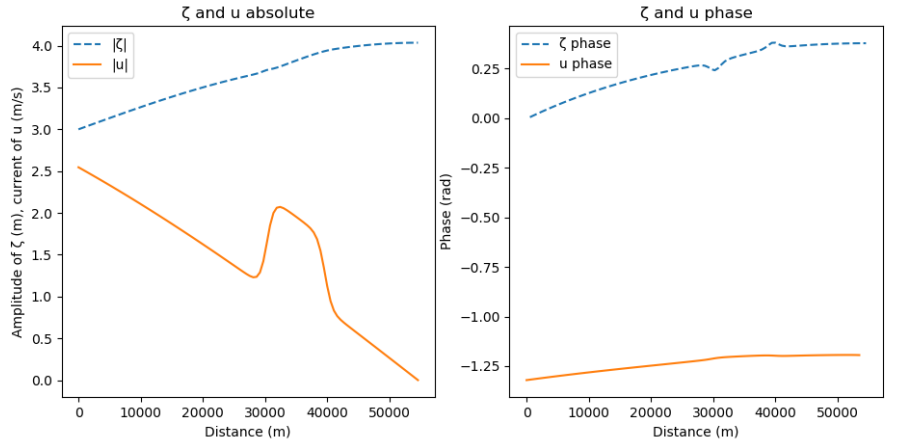


Figure 4.9: The absolute values of $\zeta$ and $u$ as calculated by the fft are displayed on the left side of the figure. In the right panel the phase of $\zeta$ and $u$ is shown as a function of the position in the estuary.

with the spatial variation of the width given by equation (4.1). A phase shift, denoted by $\phi$, can be varied between 0 and 360 degrees. In figure (4.10) snapshots are shown of the plain form of the estuary, each 1.5 hours separated from each other. The water motion at high tide (after 20 tidal cycles) is shown in fig (4.11), where the results are those obtained in paragraph 3.3. Note that at high water, the width is uniform in case of the time varying width as well, allowing for a comparison: the solutions obtained in the uniform embayment are plotted as well (dashed lines). On first sight, nothing seems to differ drastically with the results obtained in the constant embayment width B in paragraph 4.2., apart from the fact that the water level $\zeta$ is slightly higher for the case with the uniform basin. However, a closer look using the fast Fourier transform shows that higher harmonics are generated.

In figure (4.12), left panel, the fast Fourier transform of the water level $\zeta$ is displayed; the right panel shows the current $u$. The frequency of the contribution with the largest amplitude is the same for both variables as the periodic forcing with frequency $f = \sigma$, though the contribution is slightly lower compared to the time independent case. However, this figure shows that other frequencies occur, namely at $f = 2\sigma$ and $f = 3\sigma$. Even at $f = 4\sigma$, a small peak is distinguishable. The phase and amplitude of both are displayed in figure (4.13). It is clearly visible that other frequencies contribute a non-negligible amount to the total currents and water level. This measurement is once again taken at $x = 33km$. To further investigate, for each position in the embayment the fft is calculated over the latter 10 periods and displayed in a three dimensional graph. This clarifies at what positions the influence of the barrier is the highest.

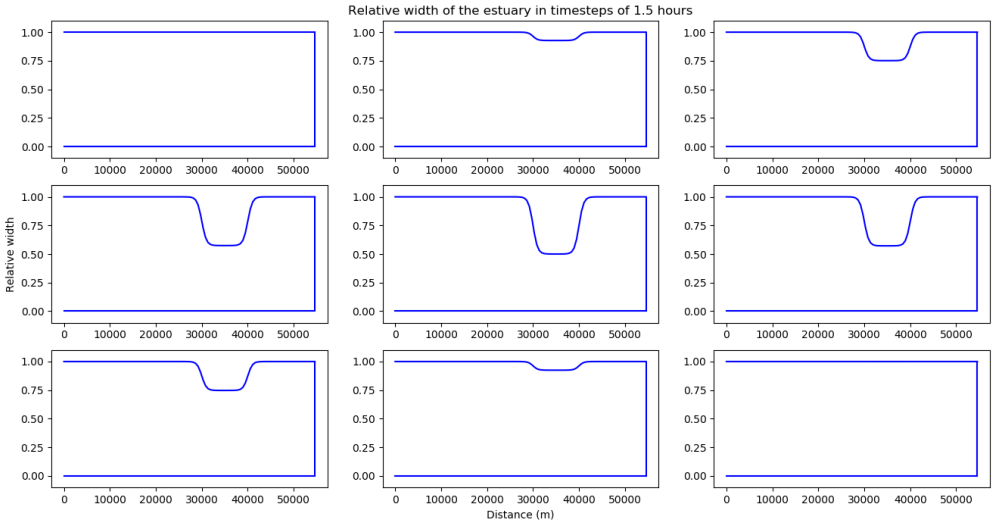


Figure 4.10: From top left to bottom right, snapshots are shown of the relative width of the embayment. The time difference between each figure is 1.5 hours. The width variations are periodic in time, with a period time of 12.25 hours. The minimum width is $\frac{1}{2}$ of its initial value.

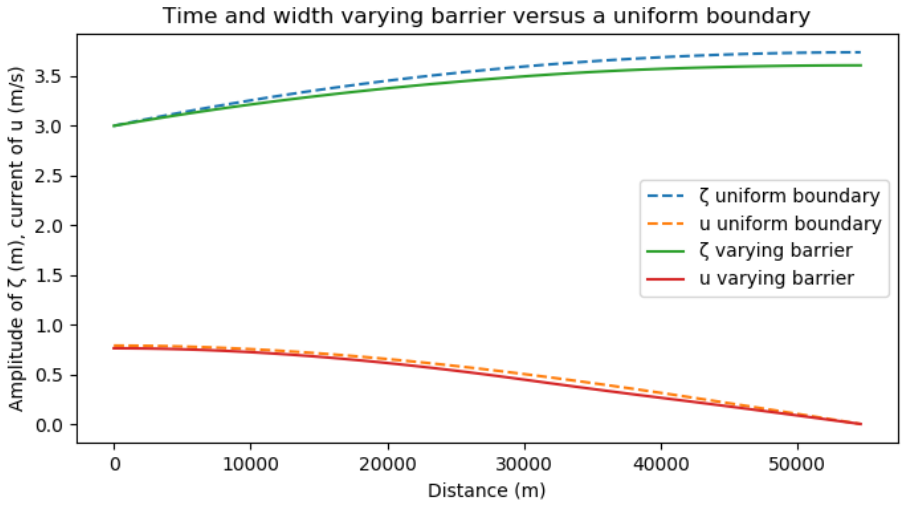


Figure 4.11: Snapshot of the estuary with the temporally and spatially dependent barrier taken after 245 hours. The water level and current are shown. The side border is back to a uniform basin at this precise time, because it is high time again. The solutions for the uniform embayment are plotted as well in dashed lines.

As it turns out, the influence of the flood barrier concerning $\zeta$ is largest at the coastline. At the inlet the amplitudes on higher frequencies have to be zero, since the amplitude at that position is prescribed and can thus not be influenced. In the middle section the amplitude of both the forcing and the higher frequency waves increases. In the next section the relative influence is discussed in detail.

Concerning the horizontal velocities $u$, the influence of the flood barrier is largest at $x = 0$, the connection with the open sea. However, also strong impacts are shown in the area in and around the barrier. The spatial disturbances of the amplitudes of the different frequencies is shown in fig (4.14) and fig (4.15) for the water level $\zeta$ and velocity $u$, respectively. In these figures, the relative frequency $\frac{f}{\sigma}$ is plotted on the x-axis, the distance to the sea at the y-axis and the amplitude at the z-axis.

From fig (4.16) in the left panel it follows that the amplitude of the water level variations for a frequency of $f = 2\sigma$ is approximately 7% of the amplitude of the main tidal constituent. The amplitudes

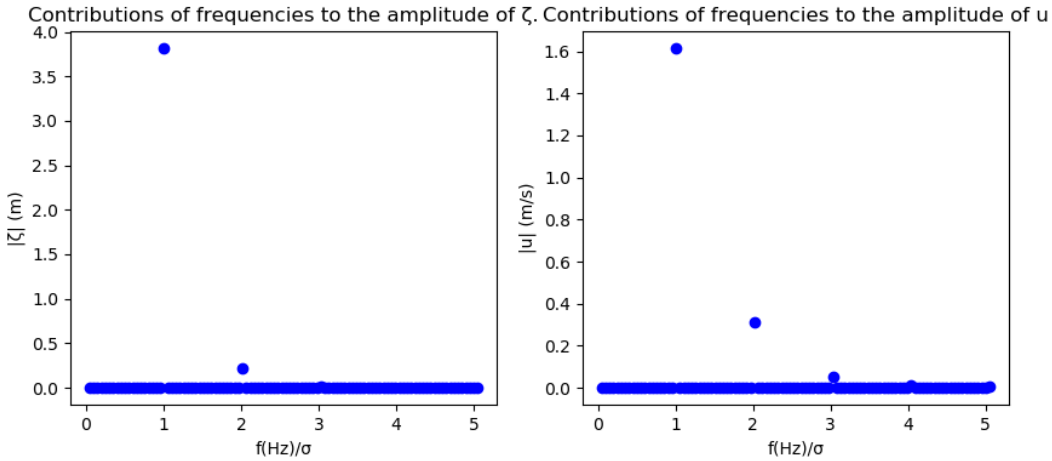


Figure 4.12: Discrete plot of the Fourier transform of the obtained solutions for $\zeta$ (left) and $u$ (right). Each dot represents the contribution to the total amplitude. The frequencies are made non-dimensional and the axis is cut off at a frequency of $f = 5\sigma$, since no other peaks were visible.

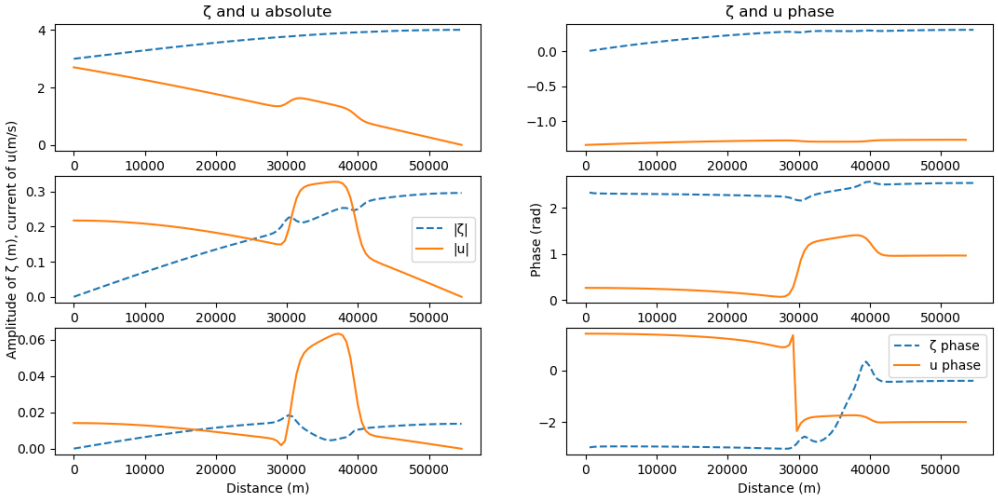


Figure 4.13: Graph of the contributions to the total water motion in the estuary with frequencies $f = \sigma$ (top), $2\sigma$ (middle) and $3\sigma$ (bottom). In the figure, $\zeta$ is shown in the left panel; $u$ is given in the right panel. This is once again measured at a position $x = 33km$, so inside the narrowing part of the basin.

belonging to the other frequencies $f = 3\sigma$ and $f = 4\sigma$ do not have a significant contribution. In the right panel the amplitude of the current $u$ is shown. This amplitude is much larger and is over 25% of the amplitude of the main constituent near the barrier. The currents with frequency $f = 3\sigma$ still have an influence inside the barrier, although the influence near the coastline and at the seaward entrance is minimal.

### 4.4.1. Sediment transport

The sediment transport *q* depends on the current velocities. More precise, $\langle u^3 \rangle$ is often used as a proxy for the sediment transport *q*, with $\langle u^3 \rangle = \frac{1}{T}\int_0^T u^3 dt$, i.e. the tidal average of $u^3$. The phase $\phi$, used to describe the width variations, given by equation (4.2), has been held zero in all experiments. In this section this phase will be varied between 0 and 360 degrees to assess the influence of this phase and the residual sediment transport *q*. This thesis provides insight on the changing behaviour of the net current when this phase is changed. For every position *x* in the embayment, the proxy for *q* is calculated and normalised via dividing by the maximum value output. In this manner the influence of

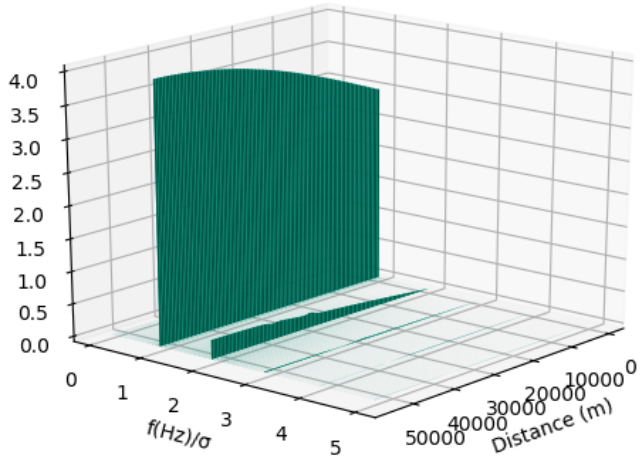


Figure 4.14: A three dimensional plot demonstrating the contribution of waves with different frequencies to the total water level $\zeta$ throughout the entire estuary. The frequency is made non-dimensional through dividing by $\sigma$.

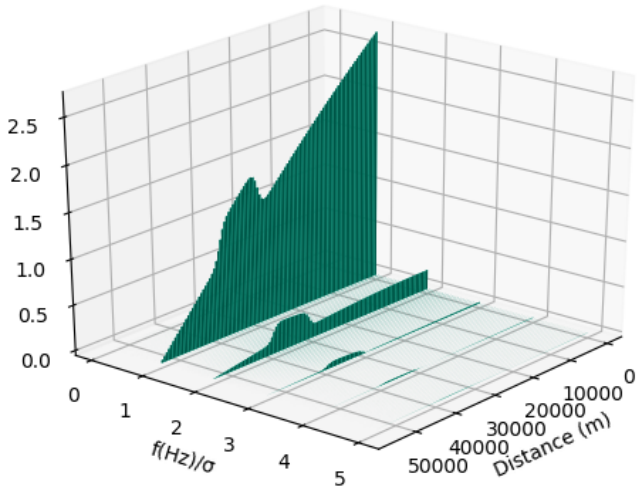


Figure 4.15: A three dimensional plot demonstrating the contribution of waves with different frequencies to the water velocity $u$ throughout the estuary. The frequency is made non-dimensional through dividing by $f = \sigma$.

the phase $\phi$ can be investigated. A negative value of $q$ means a net sediment transport out of the basin and a positive value means a landward sediment transport. From fig (4.17) it follows that for $0.2\pi \leq \phi \leq 1.4\pi$ there is a net import of sediment over the seaward boundary. Between $1.4\pi \leq \phi \leq 2.0\pi$ and $0 \leq \phi \leq 0.2\pi$, the net sediment transport at the inlet of the embayment is negative, i.e. there is a net sediment transport out of the estuary. For $1.8\pi \leq \phi \leq 2.0\pi$ and $0 \leq \phi \leq 0.1\pi$, a net seaward sediment transport is even found at all positions in the estuary.

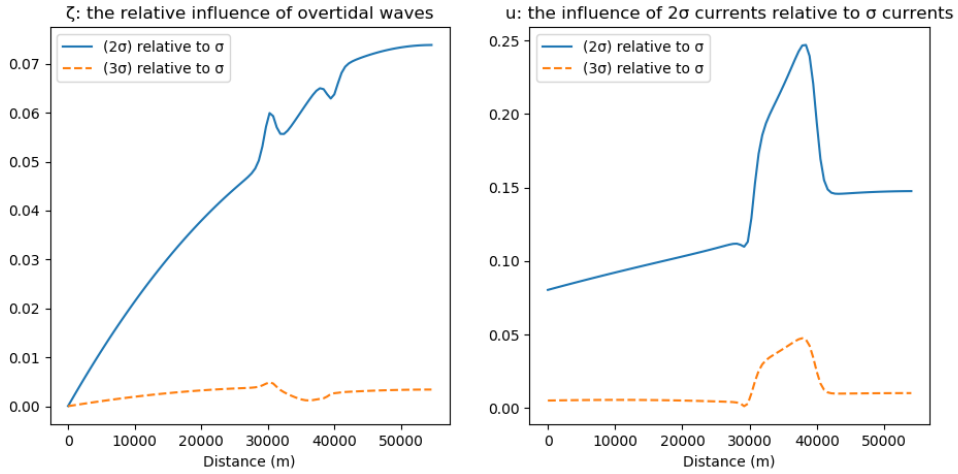


Figure 4.16: Relative influence of the water height $\zeta$ (left panel) and the currents $u$ (right panel) due to the use of the periodic barrier. The waves and currents with a frequency of $f = 2\sigma$ and $3\sigma$ are divided by the dominant effects of $\sigma$.

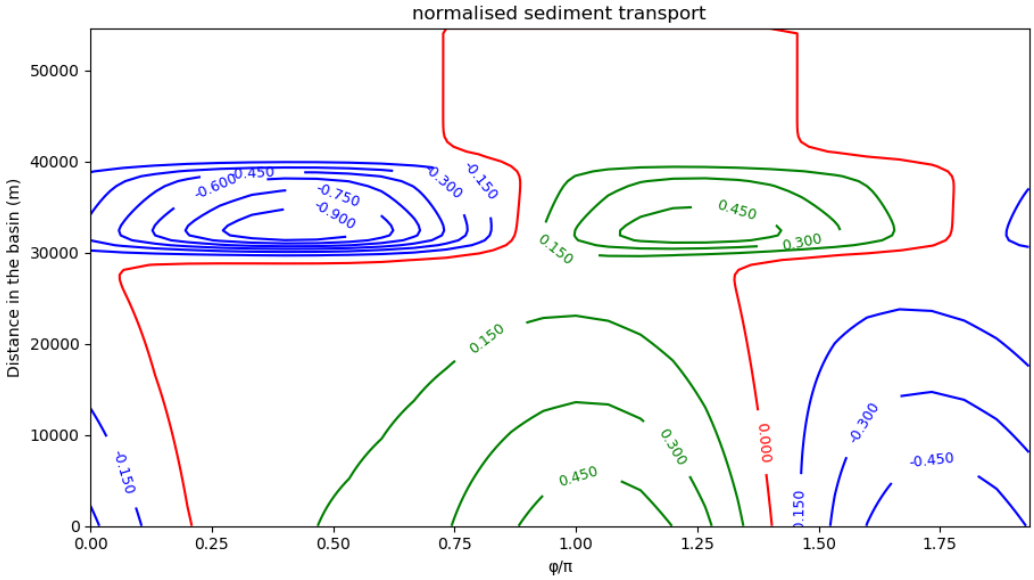


Figure 4.17: This figure shows the normalised net sediment flow at all positions of the bay for a phase shift $0 \leq \phi \leq 2\pi$. At the bottom the inlet of the estuary connected to the open sea is stationed. The coastline is positioned at the top.

# 5

# Discussion and Conclusion

## 5.1. Introduction

In this thesis, the main goal is to investigate the behaviour of the tidal dynamics and residual sediment transport in an idealized cross-sectional system: a tidal basin connected to an adjacent sea, with a time dependent barrier situated in the tidal basin. To idealize the system, the 3D Navier Stokes equations are reduced by cross-sectional averaging, resulting in a set of one dimensional shallow water equations. The bottom stress is linearised and the undisturbed water depth is considered to be uniform throughout the embayment. This thesis does not strive to give results that can be used in practise, but to give insight into the behaviour of the velocities and sediment transport and point out the possibilities for further investigation. The effects and interaction between the periodic horizontal moving time dependent barrier and the tidal forcing at the connection to the open sea is investigated. In order to approach the model the coupled system of equations is discretized. The outcome is analysed using a Fourier transform and the influence of the variant frequencies is brought to light. By varying the phase of the narrowing of the barrier compared to the tidal currents, the sedimentation can be minimized.

## 5.2. Research question

Varying the phase of the barrier over time, the sedimentation can be mapped and the main research questions can be answered.

> Q1: How does a periodic movable barrier influence the currents and water levels in an estuary driven by tidal forcing?

A periodic movable barrier which is operated on the same frequency as the tidal forcing, strongly amplifies the current inside the narrowing part of the basin. The water level does not change visibly. Moreover, the periodic width variation results in the generation of water levels variation, characterized by other frequencies; namely at frequencies $n\sigma$ with $n = 1, 2, \ldots$ For $n = 2$, the current inside the embayment at the position of the barrier contributes up to a quarter of the total current. This influence decreases rapidly with increasing $n$. The current $u$ is most affected inside the barrier region and at the open connection to the sea. The water level $\zeta$ is most affected at the coastline, however to a lesser extent than $u$.

To argue these results, equation (2.24) can be investigated. In this equation, a multiplication of (the derivative of) $\zeta(x,t)$ and $B(x,t)$ is present. Since these two variables have a forcing periodicity with frequency $f = \sigma$, an interaction should be found with double the frequency $f = 2\sigma$. This, in turn, would interfere again with the forcing frequency, and so on. This means that it is reasonable to find influences of higher generated frequencies at a multiple of $f = \sigma$, which is the case.

The second question posed in this thesis is:

> Q2: Are there manipulations to the barrier that suffices to minimize the sediment transport in the estuary?

By calculating the sediment transport at each location as a function of the phase $\phi$, the sediment transport can be systematically studied. A combination of seaward and landward transport in the estuary consequences in an accumulation of sediment, i.e. this results in estuarine turbidity maxima. Furthermore, considering that at the end of the estuary is a connection with a river stationed, a net landward flow at the coastline is not preferred either. This means that a net seaward sediment transport at all positions in the estuary is desired. A phase shift of the barrier in between $1.8\pi \leq \phi \leq 2.0\pi$ and $0 \leq \phi \leq 0.1\pi$ provides this net seaward sediment transport over the entire embayment. However, a negative sediment transport results in erosion, i.e. the regions are deepened. To prevent removal of essential ground on which the barrier is built, the deepening has to be kept small. To minimize the sedimentation while meeting the requirements, a phase shift of $\phi = 1.8\pi$ is recommended.

## 5.3. Further Research and discussion

There are a few important points that need to be discussed. First of all, as mentioned earlier, the goal of this thesis is to provide insight in the influence of a movable barrier in the qualitative behaviour of the water motion inside an estuary. As the results show, a non-negligible contribution of higher generated frequencies is measured; it is worth to look further into this subject and try different conditions. For example, the depth is taken to be constant; what effect does it have to alter this in time? The flood barrier of the Eems can be (partly) closed in two directions: the width, as discussed in this thesis, as well as the depth. There are numerous options and variations open to be explored. Another width definition of $B(x,t)$ in both amplitude, form and periodicity can be investigated.

A direct consequence of sedimentation and sludge transport is the changing water depth. The change of the bottom level in turn influences the currents and water levels inside the basin, as schematically shown in figure (5.1). This iteration is not treated in this thesis. However, it can have a strong influence on larger time scales and has to be taken into account when longer periods are considered.

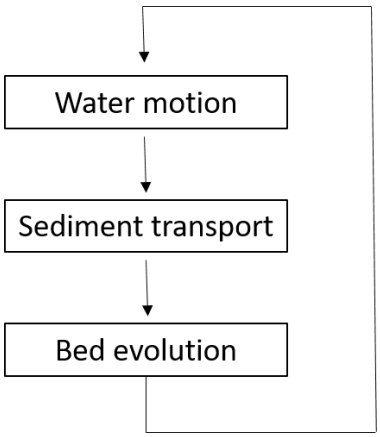


Figure 5.1: A morphodynamic loop inside an estuary. The given subjects influence each other in an iterative process.

At the edge of the barrier, i.e. at $x = 30000m$ and $x = 40000m$, small ripples are visible in the simulation with the time independent narrowing barrier. These phenomena are not explained, nor further investigated in this thesis. However, if the grid in spatial direction is finer, the ripple decreases. It was impossible to decrease the grid size further due to the limitations of the computational power.

The flood barrier starts to narrow at $x = 30000m$ and widens at $x = 40000m$, which means that the barrier has a length of 10 kilometer. Due to this extraordinary range, the behaviour inside the barrier will not blend with the phenomena at the edges and can thus be properly investigated separately. However, a side effect is that this is not a physically realistic length, which makes it hard to compare the results with values from literature. In further research an option is to zoom in on the behaviour at the edges and decrease the size of the barrier to a more realistic scenario. Also it is possible to investigate a vertically moving barrier, since this operation is possible for the Eems flood barrier too. Furthermore, the case where the barrier is nearly or even entirely closed is not included. The water motion behaves

differently and has to be approached via other methods.

# A

# Derivation of the depth averaged shallow water equations

## A.1. Leibniz integral rule

Leibniz's integral rule for differentiation under the integral sign states that for a typical integral

$$\int_{a(x,t)}^{b(x,t)} f(x,y,z,t)dz$$

the derivative can be expressed by changing the order of integration and differentiation:

$$\int_{a(x,t)}^{b(x,t)} \frac{\partial f}{\partial x}dz = \frac{\partial}{\partial x}\int_{a(x,t)}^{b(x,t)} f dz + [f]_{a(x,t)}\frac{\partial a(x,t)}{\partial x} - [f]_{b(x,t)}\frac{\partial b(x,t)}{\partial x}. \quad \text{(A.1)}$$

The same is valid considering differentiation with respect to the time:

$$\int_{a(x,t)}^{b(x,t)} \frac{\partial f}{\partial t}dz = \frac{\partial}{\partial t}\int_{a(x,t)}^{b(x,t)} f dz + [f]_{a(x,t)}\frac{\partial a(x,t)}{\partial t} - [f]_{b(x,t)}\frac{\partial b(x,t)}{\partial t}. \quad \text{(A.2)}$$

## A.2. Depth averaged conservation of mass

These derivations are all in line with the procedure presented in a thesis of M.P. Rozendaal (2019). To arrive at the depth averaged conservation of mass, one has to begin at the continuity equation:

$$\frac{\partial u}{\partial x} + \frac{\partial v}{\partial y} + \frac{\partial w}{\partial z} = 0.$$

Using the kinematic boundary conditions and the depth averaged velocities results in

$$\int_h^{H+\zeta} (\frac{\partial u}{\partial x} + \frac{\partial v}{\partial y} + \frac{\partial w}{\partial z})dz = 0,$$

where equations (2.8) and (2.9) are used. Rewriting gives

$$\int_h^{H+\zeta} (\frac{\partial u}{\partial x})dz + \int_h^{H+\zeta} (\frac{\partial v}{\partial y})dz + [w]_h^{H+\zeta} = 0.$$

Making use of Leibniz provides that

$$\frac{\partial}{\partial x}[\int_h^{H+\zeta} u dz] + \frac{\partial}{\partial y}[\int_h^{H+\zeta} v dz] + [u\frac{\partial h}{\partial x} + v\frac{\partial h}{\partial y} - w]_h - [u\frac{\partial \zeta}{\partial x} + v\frac{\partial \zeta}{\partial y} - w]_{H+\zeta} = 0. \quad \text{(A.3)}$$

Filling in boundary conditions for free surfaces:

$$\frac{\partial \zeta}{\partial t} - \frac{\partial h}{\partial t} + \frac{\partial}{\partial x}[(H+\zeta-h)\overline{u}] + \frac{\partial}{\partial y}[(H+\zeta-h)\overline{v}] = 0. \quad \text{(A.4)}$$

## A.3. Depth averaged conservation of momentum

Only the *x*-direction is considered. The *y*-direction follows the exact same procedure. In order to express the conservative form, For writing in conservative form, equation (2.6b) is added with the multiplication of equation (2.6a) by $u$, resulting in

$$\frac{\partial u}{\partial t}+\frac{\partial u^2}{\partial x}+\frac{\partial uv}{\partial y}+\frac{\partial uw}{\partial z}-fv=-\frac{1}{\rho}\frac{\partial \rho}{\partial x}+\frac{\partial}{\partial x}[\mathcal{A}_h\frac{\partial u}{\partial x}]+\frac{\partial}{\partial y}[\mathcal{A}_h\frac{\partial u}{\partial y}]+\frac{\partial}{\partial z}[\mathcal{A}_v\frac{\partial u}{\partial z}]. \tag{A.5}$$

From here on, the left hand side of this equation is elaborated first. Using the kinematic and dynamic boundary conditions provides that

$$\int_h^{H+\zeta}[\frac{\partial u}{\partial t}+\frac{\partial u^2}{\partial x}+\frac{\partial uv}{\partial y}+\frac{\partial uw}{\partial z}-fv]dz=$$

$$\frac{\partial}{\partial t}[\int_h^{H+\zeta}udz]+\frac{\partial}{\partial x}[\int_h^{H+\zeta}u^2dz]+\frac{\partial}{\partial y}[\int_h^{H+\zeta}uvdz]-f\int_h^{H+\zeta}vdz$$
$$+[u(\frac{\partial h}{\partial t}+u\frac{\partial h}{\partial x}+v\frac{\partial h}{\partial y}-w)]_h-[u(\frac{\partial \zeta}{\partial t}+u\frac{\partial \zeta}{\partial x}+v\frac{\partial \zeta}{\partial y}-w)]_{H+\zeta}=$$

$$\frac{\partial}{\partial t}[\int_h^{H+\zeta}udz]+\frac{\partial}{\partial x}[\int_h^{H+\zeta}u^2dz]+\frac{\partial}{\partial y}[\int_h^{H+\zeta}uvdz]-f\int_h^{H+\zeta}vdz.$$

Now again the averaged and its fluctuating part $\tilde{u}=u-\overline{u}$ is used, stated as

$$\int_h^{H+\zeta}\tilde{u}dz=0,$$

which results in

$$\frac{\partial}{\partial t}[\int_h^{H+\zeta}udz]+\frac{\partial}{\partial x}[\int_h^{H+\zeta}u^2dz]+\frac{\partial}{\partial y}[\int_h^{H+\zeta}uvdz]-f\int_h^{H+\zeta}vdz=$$

$$\frac{\partial}{\partial t}[(H+\zeta-h)\overline{u}]+\frac{\partial}{\partial x}[(H+\zeta-h)\overline{u}^2+\int_h^{H+\zeta}\tilde{u}^2dz]+\frac{\partial}{\partial y}[(H+\zeta-h)\overline{uv}+\int_h^{H+\zeta}\tilde{u}\tilde{v}dz]+f(H+\zeta-h)\overline{v}.$$

Integral parts are now parameterised as followed (Nihoul,1975), leading up to

$$\int_h^{H+\zeta}\tilde{u}^2dz=\tilde{\mathcal{A}_h}(H+\zeta-h)\frac{\partial \overline{u}}{\partial x},$$

and

$$\int_h^{H+\zeta}\tilde{u}\tilde{v}dz=\tilde{\mathcal{A}_h}(H+\zeta-h)\frac{\partial \overline{u}}{\partial y}.$$

This results in the total expression for the LHS:

$$(H+\zeta-h)[\frac{\partial \overline{u}}{\partial t}+\overline{u}\frac{\partial \overline{u}}{\partial x}+\overline{v}\frac{\partial \overline{u}}{\partial y}]-\frac{\partial}{\partial x}[\tilde{\mathcal{A}_h}(H+\zeta-h)\frac{\partial \overline{u}}{\partial x}]-\frac{\partial}{\partial y}[\tilde{\mathcal{A}_h}(H+\zeta-h)\frac{\partial \overline{u}}{\partial y}].$$

The hydrostatic pressure relationship, which reads as

$$p=p_a+\rho g(H+\zeta-z) \tag{A.6}$$

is used to operate the right hand side of equation (A.5). Filling in and rewriting gives:

$$\int_h^{H+\zeta}[-\frac{1}{\rho}\frac{\partial p}{\partial x}+\frac{\partial}{\partial x}(\mathcal{A}_h\frac{\partial u}{\partial x})+\frac{\partial}{\partial y}(\mathcal{A}_h\frac{\partial u}{\partial y})\frac{\partial}{\partial z}(\mathcal{A}_v\frac{\partial u}{\partial z})]dz$$

$$=-(H+\zeta-h)g\frac{\partial \zeta}{\partial x}+\frac{\partial}{\partial x}(\int_h^{H+\zeta}\mathcal{A}_h\frac{\partial u}{\partial x}dz)+\frac{\partial}{\partial y}(\int_h^{H+\zeta}\mathcal{A}_h\frac{\partial u}{\partial y}dz)$$

$$+[\mathcal{A}_h \frac{\partial u}{\partial x}\frac{\partial h}{\partial x} + \mathcal{A}_h \frac{\partial u}{\partial y}\frac{\partial h}{\partial y} + \mathcal{A}_v \frac{\partial u}{\partial z}]_h - [\mathcal{A}_h \frac{\partial u}{\partial x}\frac{\partial \zeta}{\partial x} + \mathcal{A}_h \frac{\partial u}{\partial y}\frac{\partial \zeta}{\partial y} + \mathcal{A}_v \frac{\partial u}{\partial z}]_{H+\zeta}$$

Filling in the linearised stresses (bottom and surface) gives:

$$-(H+\zeta-h)g\frac{\partial \zeta}{\partial x} + \frac{\partial}{\partial x}((H+\zeta-h)\mathcal{A}_h\frac{\partial \overline{u}}{\partial x}) + \frac{\partial}{\partial y}((H+\zeta-h)\mathcal{A}_h\frac{\partial \overline{u}}{\partial y}) + \frac{\tau_{wind,x}}{\rho} - \frac{\tau_{bx}}{\rho}$$

$$= -(H+\zeta-h)g\frac{\partial \zeta}{\partial x} + \frac{\partial}{\partial x}((H+\zeta-h)\mathcal{A}_h\frac{\partial \overline{u}}{\partial x}) + \frac{\partial}{\partial y}((H+\zeta-h)\mathcal{A}_h\frac{\partial \overline{u}}{\partial y}) - r\overline{u}$$

In total, equalling the left hand and right hand side, provides the total expression for the depth averaged conservation of momentum, resulting in

$$\frac{\partial \overline{u}}{\partial t} + \overline{u}\frac{\partial \overline{u}}{\partial x} + \overline{v}\frac{\partial \overline{u}}{\partial y} - f\overline{v} = -g\frac{\partial \zeta}{\partial x} + \frac{1}{(H+\zeta-h)}[-r\overline{u} + \frac{\partial}{\partial x}((H+\zeta-h)\mathcal{A}_h\frac{\partial \overline{u}}{\partial x}) + \frac{\partial}{\partial y}((H+\zeta-h)\mathcal{A}_h\frac{\partial \overline{u}}{\partial y})].$$

# B

# Numerical implementation

## B.1. Discretization methods

The discretizations used have a second order of convergence. The scheme of the first derivative is used in threefold: forward, central and backward. The central discretization is mostly used for positions inside the estuary. Forward and backward scheme is specifically used to cover the boundary conditions. The forward, central and backward discretizations of a given function $f(x,t)$ at position $x = j\Delta x$ and time $t = n\Delta t$ are given by

$$\frac{\partial f(j\Delta x, n\Delta t)}{\partial x} = \frac{-3f_j^n + 4f_{j+1}^n - f_{j+2}^n}{2\Delta x}, \tag{B.1a}$$

$$\frac{\partial f(j\Delta x, n\Delta t)}{\partial x} = \frac{f_{j+1}^n + f_{j-1}^n}{2\Delta x}, \tag{B.1b}$$

$$\frac{\partial f(j\Delta x, n\Delta t)}{\partial x} = \frac{3f_j^n + 4f_{j-1}^n + f_{j-2}^n}{2\Delta x}, \tag{B.1c}$$

for the spatial derivatives, respectively. The second order derivatives read

$$\frac{\partial^2 f(j\Delta x, n\Delta t)}{\partial x^2} = \frac{f_{j+2}^n - 2f_{j+1}^n + f_j^n}{(\Delta x)^2}, \tag{B.2a}$$

$$\frac{\partial^2 f(j\Delta x, n\Delta t)}{\partial x^2} = \frac{f_{j+1}^n - 2f_j^n + f_{j+1}^n}{(\Delta x)^2}, \tag{B.2b}$$

$$\frac{\partial^2 f(j\Delta x, n\Delta t)}{\partial x^2} = \frac{f_j^n - 2f_{j+1}^n + f_{j-2}^n}{(\Delta x)^2}. \tag{B.2c}$$

For the derivative with respect to time the Euler forward method is used, which reads as

$$\frac{\partial f(j\Delta x, n\Delta t)}{\partial t} = \frac{f_j^{n+1} - f_j^n}{\Delta t}. \tag{B.3}$$

## B.2. Implemented variables

The following variables are used for implementation:

- $g = 9.81$
- $H = 10$
- $c = \sqrt{gH}$
- $L = \frac{\pi c}{4\sigma} \sim 5.5 \cdot 10^4$
- $\hat{Z} = 3$

- $\sigma = \frac{2\pi}{12.25*3600}$
- $\hat{\lambda} = 1$
- $\lambda = \hat{\lambda} \cdot \sigma$
- time step size $\Delta t = 50s$
- grid size $NX = 101$, so the spatial step size $\Delta x = \frac{L}{100}$
- number of iterations $NT = 17640$

This provides that the Courant stability conditions is met, since

$$c\frac{\Delta t}{\Delta x} = 0.91 \leq 1.$$

## B.3. Implemented matrices

The implemented discretizations can be written in following form:

$$\mathbf{Z}^{n+1} = \mathcal{M} \cdot \mathbf{Z}^n + \mathbf{R}, \tag{B.4}$$

where $\mathbf{Z}^{n+1}$ denotes the solution at the next time step, $Z^n$ the obtained solution at $t = n\Delta t$. It is calculated via its part dependent on $\zeta$ and $u$, denoted by $\mathcal{M} \cdot \mathbf{Z}^n$ and its independent part $\mathbf{R}$. The obtained discretizations for the case with the temporally and spatially dependent barrier inside the estuary is given by

$$\begin{bmatrix} \zeta_0^{n+1} \\ u_0^{n+1} \\ \zeta_1^{n+1} \\ u_1^{n+1} \\ \zeta_2^{n+1} \\ u_2^{n+1} \\ \zeta_3^{n+1} \\ u_3^{n+1} \\ \vdots \end{bmatrix} = \begin{bmatrix} 0 & 0 & 0 & 0 & 0 & 0 & 0 & 0 & \dots \\ f\frac{3\Delta t}{2\Delta x}g & 1f & -f\frac{4\Delta t}{2\Delta x}g & 0 & f\frac{\Delta t}{2\Delta x}g & 0 & 0 & 0 & \dots \\ \frac{1}{2} & \frac{\Delta t}{2\Delta x}H\frac{B_0^n}{B_1^n} & 1-\frac{B_1^{n+1}}{B_1^n} & 0 & \frac{1}{2} & -\frac{\Delta t}{2\Delta x}H\frac{B_2^n}{B_1^n} & 0 & 0 & \dots \\ f\frac{\Delta t}{2\Delta x}g & f\frac{1}{2} & 0 & 0 & -f\frac{\Delta t}{2\Delta x}g & f\frac{1}{2} & 0 & 0 & \dots \\ 0 & 0 & \frac{1}{2} & \frac{\Delta t}{2\Delta x}H\frac{B_1^n}{B_2^n} & 1-\frac{B_2^{n+1}}{B_2^n} & 0 & \frac{1}{2} & -\frac{\Delta t}{2\Delta x}H\frac{B_3^n}{B_2^n} & \dots \\ 0 & 0 & f\frac{\Delta t}{2\Delta x}g & f\frac{1}{2} & 0 & 0 & -f\frac{\Delta t}{2\Delta x}g & f\frac{1}{2} & \dots \\ 0 & 0 & 0 & 0 & \frac{1}{2} & \frac{\Delta t}{2\Delta x}H\frac{B_2^n}{B_3^n} & 1-\frac{B_3^{n+1}}{B_3^n} & 0 & \dots \\ \vdots & \vdots & \vdots & \vdots & \vdots & \vdots & \vdots & \vdots & \ddots \end{bmatrix} * \begin{bmatrix} \zeta_0^n \\ u_0^n \\ \zeta_1^n \\ u_1^n \\ \zeta_2^n \\ u_2^n \\ \zeta_3^n \\ u_3^n \\ \vdots \end{bmatrix}$$

$$\begin{bmatrix} \vdots \\ \zeta_{nx-1}^{n+1} \\ u_{nx-1}^{n+1} \\ \zeta_{nx}^{n+1} \\ u_{nx}^{n+1} \end{bmatrix} = \begin{bmatrix} \ddots & \vdots & \vdots & \vdots & \vdots & \vdots & \\ \dots & 0 & 0 & \frac{1}{2} & -\frac{\Delta t}{2\Delta x}H\frac{B_{nx-1}^n}{B_{nx-2}^n} & 0 & 0 \\ \dots & 0 & 0 & -f\frac{\Delta t}{2\Delta x}g & f\frac{1}{2} & 0 & 0 \\ \dots & \frac{1}{2} & \frac{\Delta t}{2\Delta x}H\frac{B_{nx-2}^n}{B_{nx-1}^n} & 1-\frac{B_{nx-1}^{n+1}}{B_{nx-1}^n} & 0 & \frac{1}{2} & -\frac{\Delta t}{2\Delta x}H\frac{B_{nx}^n}{B_{nx-1}^n} \\ \dots & f\frac{\Delta t}{2\Delta x}g & f\frac{1}{2} & 0 & 0 & -f\frac{\Delta t}{2\Delta x}g & f\frac{1}{2} \\ \dots & 0 & -\frac{\Delta t}{2\Delta x}H\frac{B_{nx-2}^n}{B_{nx}^n} & 0 & \frac{4\Delta t}{2\Delta x}H\frac{B_{nx-1}^n}{B_{nx}^n} & 1-\frac{B_{nx}^{n+1}}{B_{nx}^n} & -\frac{3\Delta t}{2\Delta x}H \\ \dots & 0 & 0 & 0 & 0 & 0 & 1 \end{bmatrix} * \begin{bmatrix} \vdots \\ \zeta_{nx-2}^n \\ u_{nx-2}^n \\ \zeta_{nx-1}^n \\ u_{nx-1}^n \\ \zeta_{nx}^n \\ u_{nx}^n \end{bmatrix} + \mathbf{R}$$

where the top matrix denotes the left top part of the entire matrix $\mathcal{M}$; the bottom matrix gives the right end of $\mathcal{M}$. $\mathbf{R}$ denotes the terms which are not dependent on $\zeta$ or $u$, given by

$$\mathbf{R} = \begin{bmatrix} \hat{Z}\cos(\sigma\Delta t(n+1)) \\ 0 \\ H(\frac{B_1^{n+1}}{B_1^n} - 1) \\ 0 \\ H(\frac{B_2^{n+1}}{B_2^n} - 1) \\ 0 \\ H(\frac{B_3^{n+1}}{B_3^n} - 1) \\ \vdots \\ \vdots \\ H(\frac{B_{nx-2}^{n+1}}{B_{nx-2}^n} - 1) \\ 0 \\ H(\frac{B_{nx-1}^{n+1}}{B_{nx-1}^n} - 1) \\ 0 \\ H(\frac{B_{nx}^{n+1}}{B_{nx}^n} - 1) \\ 0 \end{bmatrix}.$$

The implementation of the case with the estuary with a varying, time independent, barrier is given by

$$\begin{bmatrix} \zeta_0^{n+1} \\ u_0^{n+1} \\ \zeta_1^{n+1} \\ u_1^{n+1} \\ \zeta_2^{n+1} \\ u_2^{n+1} \\ \zeta_3^{n+1} \\ u_3^{n+1} \\ \vdots \end{bmatrix} = \begin{bmatrix} 0 & 0 & 0 & 0 & 0 & 0 & 0 & 0 & \dots \\ f\frac{3\Delta t}{2\Delta x}g & 1f & -f\frac{4\Delta t}{2\Delta x}g & 0 & f\frac{\Delta t}{2\Delta x}g & 0 & 0 & 0 & \dots \\ \frac{1}{2} & \frac{\Delta t}{2\Delta x}H\frac{B_0}{B_1} & 0 & 0 & \frac{1}{2} & -\frac{\Delta t}{2\Delta x}H\frac{B_2}{B_1} & 0 & 0 & \dots \\ f\frac{\Delta t}{2\Delta x}g & f\frac{1}{2} & 0 & 0 & -f\frac{\Delta t}{2\Delta x}g & f\frac{1}{2} & 0 & 0 & \dots \\ 0 & 0 & \frac{1}{2} & \frac{\Delta t}{2\Delta x}H\frac{B_1}{B_2} & 0 & 0 & \frac{1}{2} & -\frac{\Delta t}{2\Delta x}H\frac{B_3}{B_2} & \dots \\ 0 & 0 & f\frac{\Delta t}{2\Delta x}g & f\frac{1}{2} & 0 & 0 & -f\frac{\Delta t}{2\Delta x}g & f\frac{1}{2} & \dots \\ 0 & 0 & 0 & 0 & \frac{1}{2} & \frac{\Delta t}{2\Delta x}H\frac{B_2}{B_3} & 0 & 0 & \dots \\ \vdots & \vdots & \vdots & \vdots & \vdots & \vdots & \vdots & \vdots & \ddots \end{bmatrix} * \begin{bmatrix} \zeta_0^n \\ u_0^n \\ \zeta_1^n \\ u_1^n \\ \zeta_2^n \\ u_2^n \\ \zeta_3^n \\ u_3^n \\ \vdots \end{bmatrix}$$

$$\begin{bmatrix} \vdots \\ \zeta_{nx-1}^{n+1} \\ u_{nx-1}^{n+1} \\ \zeta_{nx}^{n+1} \\ u_{nx}^{n+1} \end{bmatrix} = \begin{bmatrix} \ddots & \vdots & \vdots & \vdots & \vdots & \vdots & \\ \dots & 0 & 0 & \frac{1}{2} & -\frac{\Delta t}{2\Delta x}H\frac{B_{nx-1}}{B_{nx-2}} & 0 & 0 \\ \dots & 0 & 0 & -f\frac{\Delta t}{2\Delta x}g & f\frac{1}{2} & 0 & 0 \\ \dots & \frac{1}{2} & \frac{\Delta t}{2\Delta x}H\frac{B_{nx-2}}{B_{nx-1}} & 0 & 0 & \frac{1}{2} & -\frac{\Delta t}{2\Delta x}H\frac{B_{nx}}{B_{nx-1}} \\ \dots & f\frac{\Delta t}{2\Delta x}g & f\frac{1}{2} & 0 & 0 & -f\frac{\Delta t}{2\Delta x}g & f\frac{1}{2} \\ \dots & 0 & -\frac{\Delta t}{2\Delta x}H\frac{B_{nx-2}}{B_{nx}} & 0 & \frac{4\Delta t}{2\Delta x}H\frac{B_{nx-1}}{B_{nx}} & 1 & -\frac{3\Delta t}{2\Delta x}H \\ \dots & 0 & 0 & 0 & 0 & 0 & 1 \end{bmatrix} * \begin{bmatrix} \vdots \\ \zeta_{nx-2}^n \\ u_{nx-2}^n \\ \zeta_{nx-1}^n \\ u_{nx-1}^n \\ \zeta_{nx}^n \\ u_{nx}^n \end{bmatrix} + \mathbf{R}$$

where the top matrix again denotes the left top part of the entire matrix $\mathcal{M}$; the bottom matrix gives the right end of $\mathcal{M}$. **R** can be simplified to

$$\mathbf{R} = \begin{bmatrix} \hat{Z}\cos(\sigma\Delta t(n+1)) \\ 0 \\ 0 \\ \vdots \\ \vdots \\ 0 \\ 0 \\ 0 \end{bmatrix}.$$

The implementation considering the uniform estuary is given by

$$\begin{bmatrix} \zeta_0^{n+1} \\ u_0^{n+1} \\ \zeta_1^{n+1} \\ u_1^{n+1} \\ \zeta_2^{n+1} \\ u_2^{n+1} \\ \zeta_3^{n+1} \\ u_3^{n+1} \\ \vdots \end{bmatrix} = \begin{bmatrix} 0 & 0 & 0 & 0 & 0 & 0 & 0 & 0 & \dots \\ f\frac{3\Delta t}{2\Delta x}g & 1f & -f\frac{4\Delta t}{2\Delta x}g & 0 & f\frac{\Delta t}{2\Delta x}g & 0 & 0 & 0 & \dots \\ \frac{1}{2} & \frac{\Delta t}{2\Delta x}H & 0 & 0 & \frac{1}{2} & -\frac{\Delta t}{2\Delta x}H & 0 & 0 & \dots \\ f\frac{\Delta t}{2\Delta x}g & f\frac{1}{2} & 0 & 0 & -f\frac{\Delta t}{2\Delta x}g & f\frac{1}{2} & 0 & 0 & \dots \\ 0 & 0 & \frac{1}{2} & \frac{\Delta t}{2\Delta x}H & 0 & 0 & \frac{1}{2} & -\frac{\Delta t}{2\Delta x}H & \dots \\ 0 & 0 & f\frac{\Delta t}{2\Delta x}g & f\frac{1}{2} & 0 & 0 & -f\frac{\Delta t}{2\Delta x}g & f\frac{1}{2} & \dots \\ 0 & 0 & 0 & 0 & \frac{1}{2} & \frac{\Delta t}{2\Delta x}H & 0 & 0 & \dots \\ \vdots & \vdots & \vdots & \vdots & \vdots & \vdots & \vdots & \vdots & \ddots \end{bmatrix} * \begin{bmatrix} \zeta_0^{n} \\ u_0^{n} \\ \zeta_1^{n} \\ u_1^{n} \\ \zeta_2^{n} \\ u_2^{n} \\ \zeta_3^{n} \\ u_3^{n} \\ \vdots \end{bmatrix}$$

$$\begin{bmatrix} \vdots \\ \zeta_{nx-1}^{n+1} \\ u_{nx-1}^{n+1} \\ \zeta_{nx}^{n+1} \\ u_{nx}^{n+1} \end{bmatrix} = \begin{bmatrix} \ddots & \vdots & \vdots & \vdots & \vdots & \vdots & \\ \dots & 0 & 0 & \frac{1}{2} & -\frac{\Delta t}{2\Delta x}H & 0 & 0 \\ \dots & 0 & 0 & -f\frac{\Delta t}{2\Delta x}g & f\frac{1}{2} & 0 & 0 \\ \dots & \frac{1}{2} & \frac{\Delta t}{2\Delta x}H & 0 & 0 & \frac{1}{2} & -\frac{\Delta t}{2\Delta x}H \\ \dots & f\frac{\Delta t}{2\Delta x}g & f\frac{1}{2} & 0 & 0 & -f\frac{\Delta t}{2\Delta x}g & f\frac{1}{2} \\ \dots & 0 & -\frac{\Delta t}{2\Delta x}H & 0 & \frac{4\Delta t}{2\Delta x}H & 1 & -\frac{3\Delta t}{2\Delta x}H \\ \dots & 0 & 0 & 0 & 0 & 0 & 1 \end{bmatrix} * \begin{bmatrix} \vdots \\ \zeta_{nx-2}^{n} \\ u_{nx-2}^{n} \\ \zeta_{nx-1}^{n} \\ u_{nx-1}^{n} \\ \zeta_{nx}^{n} \\ u_{nx}^{n} \end{bmatrix} + \mathbf{R}$$

where the top matrix again denotes the left top part of the entire matrix $\mathcal{M}$; the bottom matrix gives the right end of $\mathcal{M}$. **R** yields the same simplification considering the spatially varying barrier, given by

$$\mathbf{R} = \begin{bmatrix} \hat{Z}\cos(\sigma\Delta t(n+1)) \\ 0 \\ 0 \\ \vdots \\ \vdots \\ 0 \\ 0 \\ 0 \end{bmatrix}.$$

# Bibliography


F.S. Acton. *Numerical methods that work*. Harper & Row, 1970.

M.B. Van Gijzen C. Vuik, F.J. Vermolen and M.J. Vuik. *Numerical Methods for Ordinary Differential Equations*. Delft Academic Press, Delft, 2018.

W.M. Cameron and D. Pritchard. *Estuaries*. John Wiley and Sons, 1963.

B. Cushman-Roisin and J.M. Beckers. *Introduction to Geophysical Fluid Dynamics*. Academic Press, 2010.

H.E. de Swart. *Physics of coastal systems*. Utrecht University, 2009.

H.J. de Vriend et al. *Coastal inlets and tidal basins*. TU Delft, 2002.

C.T. Friedrichs and O.S. Madsen. *Nonlinear Diffusion of the Tidal Signal in Frictionally Dominated Embayments*. Journal of Geophysical Research, 1992.

Theo Gerkema. *An Introduction to Tides*. Cambridge University Press, 2019.

R. Haberman. *Applied Partial Differential Equations*. Pearson Education, 5th edition, 2014.

J. C. J. Nihoul. *Modelling of Marine Systems*. Elsevier Scientific Publishing Company, 1975.

J. Pedlosky. *Geophysical Fluid Dynamics*. Springer-Verlag New York, 1987.

W.H. Press. *Numerical Recipes in C*. Cambridge University Press, 1988.

H.M. Schuttelaars. *Evolution and Stability Analysis of Bottom Patterns in Tidal Embayments*. Utrecht University, 1997.

H.M. Schuttelaars and H.E. De Swart. *An idealized long-term morphodynamic model of a tidal embayment*. European Journal of Mechanics, 1996.

C.B. Vreugdenhil. *Numerical methods for shallow-water flow*. Springer Science+business media, 1994.